DO VIBRATIONAL SPECTROSCOPIES UNIQUELY DESCRIBE PROTEIN DYNAMICS?

The Case for Myoglobin

WILLIAM BIALEK*‡ AND ROBERT F. GOLDSTEIN*§

*Department of Biophysics and Medical Physics, and Biology and Medicine Division, Lawrence Berkeley Laboratory, University of California, Berkeley, California 94720; ‡Institute for Theoretical Physics, University of California, Santa Barbara, California 93106; and §Department of Cell Biology, Sherman Fairchild Center, Stanford University School of Medicine, Stanford, California 94305

ABSTRACT We develop a quasi-harmonic description of protein dynamics and apply this description to the anomalous Mössbauer, infrared, x-ray diffraction, and EXAFS (extended x-ray absorption fine structure spectroscopy) data that are available for myoglobin (Mb) and its interactions with carbon monoxide (CO). In the quasi-harmonic approximation the dynamical parameters derived from these spectroscopic data are relevant in the calculation of reaction rates, and we give a quantitative description of the nonexponential kinetics of Mb–CO binding observed at low temperatures. All these data have previously been interpreted in terms of the more complex conformational substates model for protein dynamics. We point out several problems with this model and propose experiments that can provide detailed tests of the quasi-harmonic theory proposed here.

INTRODUCTION

A large number of experiments and computer simulations have made it clear that proteins are dynamic systems whose structures fluctuate over a wide range of time and amplitude scales (1–4). What is not clear is how these structural fluctuations are related to the biological function of proteins, particularly with regard to the determination and control of chemical reaction rates (5–9). Indeed it is not clear that structural fluctuations on a picosecond time scale have any relevance at all to biochemical phenomena on a millisecond time scale, except perhaps for their entropic contribution to the thermodynamics of proteins and protein/ligand interactions (10–12).

In this paper we formulate a theoretical approach that links dynamics and function. In particular we show how the parameters of protein dynamics derived from spectroscopic experiments can be used more or less directly in calculations of biochemical reaction rates. This approach is illustrated by an analysis of Mössbauer, infrared, x-ray diffraction, and EXAFS data on myoglobin (Mb) and its interaction with carbon monoxide (CO), and we find that the parameters derived from this analysis allow a quantitative interpretation of the nonexponential kinetics of Mb–CO binding at low temperatures (5).

Our approach is a "quasi-harmonic" theory of protein dynamics (13) and leans heavily on theoretical methods used in describing the dynamics of solids and other interacting many-body systems (14–18). An essential aspect of this many-body method is not so much its calculational power, but rather a demonstration that complicated interactions among a large number of atoms can be described by a simple physical picture. This picture, which we contrast with other views of protein dynamics, such as the conformational substates model derived from previous analyses of the myoglobin data (4), leads us to a number of quantitative predictions regarding myoglobin dynamics that can be tested by high resolution spectroscopy.

BASIC FEATURES OF A QUASI-HARMONIC THEORY

Even a relatively small protein has a very large number of degrees of freedom, and the first step in any theory of protein dynamics is to separate these degrees of freedom into manageable subsets; the first such separation is between electronic and vibrational coordinates. Our approach to the electronic/vibrational separation is purely phenomenological (19, 20): we call the electronic states those states whose population one actually measures, for example in a kinetic experiment.[1] Reactants and products

Please address correspondence to W. Bialek at the Institute for Theoretical Physics.

‡ and § are present addresses.

[1] In formal quantum mechanical terms this means that we choose the electronic states as the eigenstates of the measurement operator in the kinetic experiment, and call all the remaining degrees of freedom that commute with the measurement operator (and which are required to form a complete set of observables) "vibrational." This strict application of quantum measurement theory (21) becomes a bit more phenomenological

in a chemical reaction are identified with two electronic states, and methods that have been developed for computing electronic transition rates can be applied to the calculation of reaction rates.

Within a single electronic state the vibrational degrees of freedom may be described by a set of atomic coordinates $\{q_\alpha\}$, associated momenta $\{p_\alpha\}$, and masses m_α. The energy of the system (Hamiltonian) is

$$H = \sum_\alpha \frac{p_\alpha^2}{2m_\alpha} + V(\{q_\alpha\}), \tag{1}$$

where the function $V(\{q_\alpha\})$ defines the multi-dimensional "potential surface" on which the protein moves. Possible cross-sections through this surface are shown in Fig. 1.

The simplest possibility is that the surface is parabolic, as in Fig. 1 *a*, which corresponds to the harmonic approximation. If this is true then there exists a set of normal coordinates $Q_\alpha = \Sigma_\beta A_{\alpha\beta} q_\beta$, associated with vibrational frequencies ω_α, and the Hamiltonian becomes

$$H = \frac{1}{2}\sum_\alpha [(dQ_\alpha/dt)^2 + \omega_\alpha^2 Q_\alpha^2]. \tag{2}$$

In terms of these coordinates the dynamics of the system is simple and straightforward, both in classical mechanics and in quantum mechanics (22, 23).

The harmonic approximation cannot, however, be exact. Empirically the potential surfaces that describe protein dynamics are not parabolic (2). A number of experiments, particularly on myoglobin, seem inconsistent with the predictions of the harmonic approximation, and this has led to the development of alternative theories (4), such as the conformational substates model schematized in Fig. 1 *b*. If we take Eq. 2 seriously as the definition of the harmonic approximation then there is an even more serious problem, since this Hamiltonian predicts that energy placed in one normal mode lives forever, never being transferred to other modes or dissipated to the solvent that surrounds the protein.

In spite of these difficulties the harmonic approximation remains attractive, not least because of its calculational simplicity. Recent molecular dynamics simulations (24, 25) demonstrate that if one simply assumes the potential surface to be parabolic, with a curvature equal to that at the minimum, one can reproduce with reasonable accuracy the root-mean-square fluctuations in atomic positions as calculated from a full anharmonic potential surface.

It is convenient to think about the harmonic approximation in quantum mechanical terms. The energy levels of mode α are then $\hbar\omega_\alpha(n + 1/2)$, with n an integer, and the nth level may be described as a state in which n phonons (vibrational quanta) are present. When we use the harmonic approximation we are assuming that if many phonons are excited in the protein then these phonons will not interact with one another, and the success of harmonic calculations in reproducing molecular dynamics simulations suggests that the neglect of phonon-phonon interactions is not as serious as one might have expected.

There are in fact several examples in many-body physics where a collection of anharmonically interacting particles can be described by a nearly noninteracting "gas" of quanta termed quasi-particles. A case in point are the electrons in a heavy atom: one can describe these atoms by a simple shell structure, making use of one-electron orbitals and the Pauli principle, this being true in spite of the fairly strong Coulomb interactions among the electrons. Similar comments could be made regarding the electrons in a solid, the shell model of the nucleus, and the quantum fluids ^{3}He and ^{4}He at low temperatures (for review see references 14–18). It should be emphasized that calculations of the ground or equilibrium state for these systems may involve the complexity of the full anharmonic interactions, but for excitations above the equilibrium state that determine the system dynamics a quasi-particle gas forms a good approximation.

These results in many-body theory suggest a *quasi-harmonic approximation* for protein dynamics in which there exist weakly interacting phonons, although these phonons might not be the normal modes calculated in the harmonic approximation. Intuitively, these quasi-harmonic phonons can be constructed as normal modes in the average potential that the protein experiences during its time evolution. On the real potential surface the local curvature is a function of the protein coordinates and hence fluctuates as these coordinates fluctuate; we would like to choose normal modes that are defined by the average value of this curvature. In fact this must be done self-consistently, since the fluctuations in coordinates are themselves determined by the normal mode structure, and it is necessary to include corrections to this simple "self-consistent field." This procedure is formalized in Appendix A, where we collect the basic formulae used in the calculations below.

A simple example is provided by the potential surface of Fig. 1 *c*; potentials of this qualitative form arise from many different microscopic interactions (van der Waals, hydrogen bonding, etc.). Applying the quasi-harmonic approximation one finds that the quasi-normal modes have an equilibrium position that shifts toward the "soft" direction at higher temperatures, which is essentially a description of thermal expansion, and that the normal mode frequency decreases with increasing temperature, corresponding to the fact that the molecule samples regions of smaller curvature at higher energies (temperatures). Thermal expansion and mode softening are not artifacts of the quasi-harmonic approximation; rather they are features of the exact dynamics of the system on the fully anharmonic potential surface. The important point is that these phe-

when we realize that most spectroscopic probes of proteins are sensitive to both electronic and vibrational degrees of freedom if we define these using a more conventional separation method.

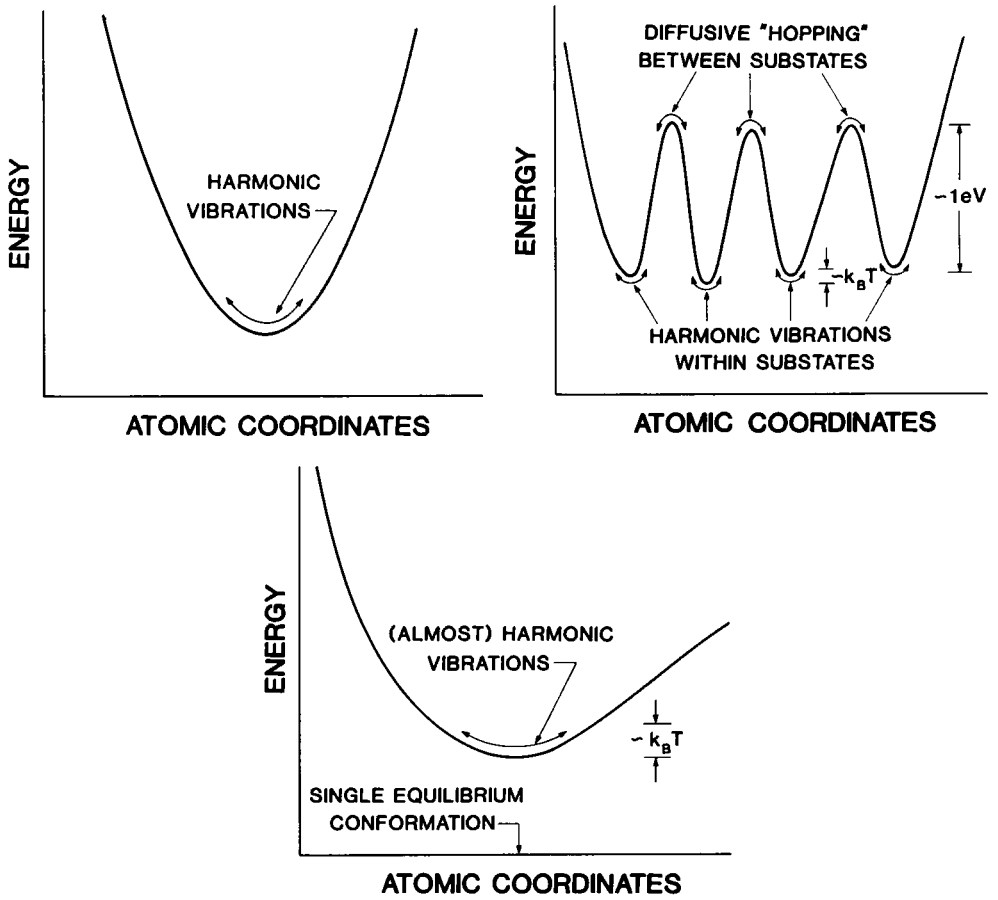

FIGURE 1. Three models of protein dynamics, as described in the text: (*a*) the harmonic approximation; (*b*) conformational substates after reference 4; and (c) the quasi-harmonic theory advocated here.

nomena, which occur only in anharmonic systems, can be described within the quasi-harmonic approximation. Indeed one way of defining the quasi-harmonic approximation is just to demand that it correctly describe these two features of the anharmonic dynamics, as may be seen from Appendix A.

Whereas a classical harmonic coordinate undergoes a mean-square displacement that grows linearly with temperature, in the quasi-harmonic approximation to the system schematized in Fig. 1 *c* the mean-square displacement grows more rapidly. The opposite situation—mean-square displacement grows less than linearly with T—can result in the quasi-harmonic approximation either from quantum effects or from potential surfaces with "hard walls." Thus while the observation of nonlinear temperature dependences for the mean-square atomic displacements in a protein would invalidate the classical harmonic approximation, it is perfectly consistent with the quasi-harmonic theory advocated here.

While the dynamics of a protein are fairly simple when described in terms of the quasi-normal modes, they are not simple if we follow a small group of atoms. The motion of any single atom consists of a superposition of many modes and hence need not have any simple temporal structure; this point is important in attempts to define the effective viscosity of the protein interior using molecular dynamics simulations (1–4), as discussed below. Again we appeal to analogies with other many-body systems: if we follow individual electrons in a metal we find quite a complex picture, but by transforming to the quasi-particle representation this picture simplifies enormously (14–18).

The quasi-normal modes have a large range of frequencies and "wavelengths," from high frequency, localized vibrations of neighboring atoms to low frequency breathing motions that can involve a large fraction of the atoms in the protein. Motions of different modes are independent, but motions of individual atoms are not; in particular, it is possible to have modes that give rise to correlated motions of widely separated atoms, and in this way motions in the interior of the protein can be affected by solvent interactions at the protein surface.[2]

The quasi-harmonic approximation is easily generalized to describe the interactions between the protein and the surrounding solvent, as formalized in Appendix B. For

[2]The long wavelength, low-frequency vibrational modes thus provide a natural language for discussing long-range interactions in proteins, such as those involved in allostery.

each instantaneous configuration of the solvent we define a full quasi-harmonic dynamics of the protein; as the solvent configuration fluctuates the parameters of this dynamics—the equilibrium positions, mode frequencies, and mode structures—will fluctuate. If the fluctuations are on time scales comparable to the mode frequencies ω_α then the protein can transfer energy to the solvent and exhibit vibrational relaxation at a rate γ_α; in this sense the solvent provides a "heat bath" that interacts with the protein and allows it to come to thermal equilibrium. If the solvent fluctuations are on a much slower time scale one can observe them directly, for example as inhomogeneous broadening of the vibrational spectra (26).

One important class of solvent molecules forms a shell bound to the protein surface; in myoglobin and other medium-size proteins there are approximately 100 "bound waters" (27, 28). At room temperature these waters exchange among the available sites (and presumably with the bulk solvent) on a nanosecond time scale (29). This time is long compared to the vibrational frequencies and relaxation times, so that in infrared or Raman spectroscopy the solvent shell contributes to (and in some systems dominates) the inhomogeneous broadening. If a large number of solvent molecules contribute to the inhomogeneous broadening then by the central limit theorem the resulting frequency distribution will be Gaussian, and this is the case even in fairly simple molecular liquids (26).

The time scale for solvent shell exchange is, however, much shorter than typical chemical reaction times, so the biochemical behavior of a protein at room temperature reflects an average over the different solvent shell configurations and hence over the distribution of vibrational frequencies, etc. This ceases to be true in frozen solution, where the time for exchange among solvation sites becomes very long and the protein cannot average over its inhomogeneous vibrational frequency distribution. Each protein molecule is essentially stuck with a particular set of vibrational frequencies chosen randomly from the inhomogeneous distributions.

MÖSSBAUER SPECTRA

The Mössbauer spectrum of the iron atom in myoglobin is sensitive to the motion of this single atom and is independent of correlations between the motion of the iron atom and its neighbors. This single-atom sensitivity is unique to the Mössbauer effect as a spectroscopic probe of protein dynamics. The Mössbauer spectrum of a simple nucleus, centered at energy E_0 and having natural linewidth Γ, is given by (30)

$$I(E) = \frac{1}{2\pi\hbar}\int_{-\infty}^{+\infty} d\tau e^{i(E-E_0)\tau/\hbar - \Gamma|\tau|/2}\langle e^{i\mathbf{k}\cdot\mathbf{x}(\tau)} e^{-i\mathbf{k}\cdot\mathbf{x}(0)}\rangle, \quad (3)$$

where $\mathbf{k}$ is the wavevector of the Mössbauer radiation, $\langle\cdots\rangle$ denotes an average over the ensemble of atoms in the sample, and $\mathbf{x}(\tau)$ is the (vector) position of the nucleus; the spectrum is normalized so that if there is no motion of the nucleus then $\int_{-\infty}^{+\infty} dE I(E) = 1$.

In the quasi-harmonic approximation the position of the iron atom may be written as

$$\mathbf{x}(\tau) = \sum_{\alpha=1}^{N} \mathbf{A}_\alpha(\mathrm{Fe})\tilde{Q}_\alpha(\tau),$$

where the $\tilde{Q}_\alpha$ are the quasi-normal coordinates, the $\mathbf{A}_\alpha(\mathrm{Fe})$ are a set of transformation coefficients, and we have assumed that N modes make significant contributions. As discussed in Appendix A, the essential mathematical feature of the quasi-harmonic approximation is that each $\tilde{Q}_\alpha(t)$ is an independent Gaussian random variable. Correlation functions involving iron atom position, as in Eq. 3, can therefore be written in terms of the elementary correlation functions $\langle\tilde{Q}_\alpha(\tau)\tilde{Q}_\alpha(0)\rangle$ for each mode. To obtain the correct low temperature behavior we must treat the quasi-normal coordinates quantum mechanically, but the same principles apply (see Appendix A and reference 20): the Mössbauer spectrum of the iron atom can be written in terms of elementary correlation functions for the quasi-normal modes, and these are uniquely determined by the frequencies ω_α and damping constants γ_α. We find

$$\begin{aligned} I(E) = &\int dE' \int d\Omega_1 \int d\Omega_2 \cdots \int d\Omega_N \\ &\times \delta(E - E' - \hbar\Omega_1 - \hbar\Omega_2 - \cdots - \hbar\Omega_N) \\ &\times I(E'; \mathbf{x} = 0)\, F_1(\Omega_1) F_2(\Omega_2) \cdots F_N(\Omega_N), \end{aligned} \quad (4)$$

where $I(E; \mathbf{x} = 0)$ is the spectrum in the absence of atomic motion,

$$I(E; \mathbf{x} = 0) = \frac{1}{\pi}\frac{\hbar\Gamma}{(E - E_0)^2 + (\hbar\Gamma)^2}, \quad (5)$$

and the spectral function of each mode is given by

$$\begin{aligned} F_\alpha(\Omega) &= \frac{1}{2\pi}\int_{-\infty}^{+\infty} d\tau e^{+i\Omega\tau}\langle e^{iS_\alpha^{1/2}\tilde{Q}_\alpha(\tau)} e^{-iS_\alpha^{1/2}\tilde{Q}_\alpha(0)}\rangle \\ &= \frac{1}{\pi} e^{-S_\alpha(2\bar{n}_\alpha+1)} \sum_{n=0}^{\infty}\sum_{m=0}^{\infty} \frac{S_\alpha^{n+m}(\bar{n}_\alpha+1)^n \bar{n}_\alpha^m}{n!m!} \\ &\quad\times \frac{\gamma_\alpha(n+m)}{[\Omega - (n-m)\omega_\alpha]^2 + \gamma_\alpha(n+m)^2}, \end{aligned} \quad (6)$$

where

$$S_\alpha = \frac{\hbar}{2\omega_\alpha}[\mathbf{k}\cdot\mathbf{A}_\alpha(\mathrm{Fe})]^2$$

is a dimensionless coupling constant describing the contribution of mode α to the spectrum and $\bar{n}_\alpha = (e^{\hbar\omega_\alpha/k_BT} - 1)^{-1}$ is the average number of phonons in mode α at absolute temperature T.

Eq. 6 allows us to classify contributions from different types of modes. For any individual mode that makes a small contribution to the iron atom motion, corresponding to a small $|\mathbf{A}_\alpha(\mathrm{Fe})|$, the double sum in Eq. 6 collapses to

those terms with $n = m = 0$. These terms are proportional to delta functions of the frequency and thus cannot change the structure of the spectrum although they contribute a constant attenuation. In particular, the contribution of any single acoustic mode (sound wave) in the myoglobin crystal is $|\mathbf{A}_\alpha| \sim N^{-1/2}$, where N is the number of unit cells in the whole crystal. The effect of the acoustic modes is therefore only to attenuate the Mössbauer spectrum but not to change its shape; this attenuation is discussed in Appendix C.

A second class of modes whose contribution can be simplified are the high frequency, localized vibrations of the iron atom relative to its near neighbors. These modes have $\bar{n}_\alpha \approx 0$, and thus only terms with $m = 0$ can contribute to the sum in Eq. 6. Terms with $m = 0$ and $n \neq 0$, however, are shifted by $n\omega_\alpha$ away from the center frequency of the spectrum, and unless one has low frequency modes that contribute ~1 Å to the root-mean-square motion of the iron atom at absolute zero this shift cannot be compensated. In the true recoilless Mössbauer spectrum (that part of the spectrum in a small neighborhood about E_0) high frequency modes therefore contribute only through the $m = n = 0$ terms in Eq. 6. As with the acoustic modes this contribution provides only a constant attenuation; in the case of the high frequency modes this attenuation is temperature-independent. We thus see that in the quasi-harmonic approximation dynamical effects on the structure of the Mössbauer spectrum are significant *only* for low frequency modes that are strongly coupled to the iron atom displacement, and it is important to note that inhomogeneous broadening of these modes has no effect on the structure of the spectrum.

The structure of the myoglobin molecule is suggestive of a very important class of low frequency modes, the breathing modes of the F alpha helix. The iron atom is attached to the protein through a histidine group at the end of this $L \sim 1.2$ nm alpha-helical segment. One of the lowest frequency modes of the helix is the uniform stretching mode, whose properties may be understood (31) by taking the alpha helix to be a uniform elastic rod of area $A = 5 \times 10^{-19}$ m^2, density $\rho = 1.3 \times 10^3$ kg/m^3, and Young's modulus $Y = 2 \times 10^{10}$ N/m^2. The stretching motion is resisted by a stiffness $\kappa = YA/L = 8.3$ N/m and involves a mass $m = \rho AL = 7.8 \times 10^{-25}$ kg, determining a mode frequency $\omega = (\kappa/m)^{1/2} = 2\pi\,(5.1 \times 10^{11}\ \mathrm{s}^{-1})$; $\hbar\omega = 17\ \mathrm{cm}^{-1}$. The normal coordinate associated with this mode[3] is $\tilde{Q} = m^{1/2}\delta L$, where δL denotes the deviation of the helix length from its equilibrium value. Light scattering experiments on alpha-helical polymers (32) have shown that these low frequency modes have rather small vibrational relaxation rates, $\gamma \sim 10^9\ \mathrm{s}^{-1}$; $\hbar\gamma \sim 0.005\ \mathrm{cm}^{-1}$, even at room temperature.[4]

The stiffness of the iron-histidine bond, as determined from the Fe-His vibrational frequency (33), is much greater than the stiffness of the F helix calculated above. As the helix changes its length by δL the iron atom will thus also undergo a displacement of approximately δL; the magnitude of the coefficient $\mathbf{A}_\alpha(\mathrm{Fe})$ is therefore $|\mathbf{A}| = m^{-1/2}$ for this mode, and the coupling constant is

$$S_\alpha = \frac{\hbar}{2\omega_\alpha}[\mathbf{k}\cdot\mathbf{A}_\alpha(\mathrm{Fe})]^2 = \frac{4\pi^2\hbar}{2m\omega\lambda^2}\cos^2\theta = (0.13)\cos^2\theta,$$

where $\lambda = 8.6 \times 10^{-11}$ m is the wavelength of the Mössbauer radiation and θ is the angle between the propagation of the radiation and the axis of the iron atom motion in this mode.

Consider the simplest analysis, including just this one low-frequency mode of the helix. The Mössbauer spectrum becomes

$$I(E) = \frac{1}{\pi}\int_{-1}^{1} \mathrm{d}(\cos\theta)A(\theta,T)\exp[-0.13(2\bar{n}+1)\cos^2\theta]$$
$$\times \sum_{m=0}^{\infty}\frac{[(0.13)^2\bar{n}(\bar{n}+1)\cos^2\theta]^m}{(m!)^2}\frac{2m\gamma}{(E-E_0)^2+(\Gamma+2m\gamma)^2}, \quad (7)$$

where with ω from above we find $\bar{n} = [\mathrm{e}^{-(25\mathrm{K})/T} - 1]^{-1}$ and we have averaged over the orientation of the wavevector to simulate the random powder spectrum appropriate to the polycrystalline samples used in the myoglobin experiments (34–37). $A(\theta, T)$ collects the temperature- and possibly orientation-dependent attenuation factors that arise from the acoustic and high-frequency modes. Because of the orientational averaging it is impossible to predict the details of the spectrum;[5] most of the data have been collected on myoglobin and myoglobin derivatives that have nontrivial magnetic states, leading to further complications in the spectrum. Nonetheless, some features of the theory are clear:

(*a*) The spectrum consists of a single Lorentzian term at temperatures such that $(0.13)^2\bar{n}(\bar{n}+1) \ll 1$, which is $T \ll$

[3]In making these simple identifications we are really using the strict harmonic, rather than the quasi-harmonic approximation. We therefore expect that our parameter estimates will not be exact, but they should be approximately correct. Note also that in the passage from harmonic to quasi-harmonic approximations some of these parameters can acquire a temperature dependence, as described above.

[4]Since this rather small relaxation rate is found in a model system, some justification is required in applying it to Mb. The experiments, done on both dry and hydrated material, indicate that the dominant contribution to the phonon lifetime is from decay processes internal to the helix, presumably the breakup of one phonon into two. Because the helix is effectively one-dimensional, the frequency and temperature dependence of these processes is much less than that in ordinary three-dimensional crystals and the slowness of the relaxation rate is not the result of complex selection rules that would be broken in the protein environment. This breakup process is quenched if we consider the lowest frequency modes of the helix, as done here. The only remaining decay processes are then anharmonic interactions among the different structural domains and dissipation through the small helix/solvent contact region. We see no reason to doubt that the long phonon lifetimes observed in alpha-helical polymers *could* be relevant to the dynamics of globular proteins.

[5]In fact this problem plagues any interpretation of the spectrum that does not assume either isotropic or uniaxial motion.

200 K. This term arises from the conventional Mössbauer process in which the nucleus absorbs the incident radiation without the absorption or emission of any phonons.

(*b*) At temperatures above 200 K the spectrum will break into multiple Lorentzians, with the first anomalous component having a width $2\gamma \sim 10^9\ s^{-1}$. This term arises from a modified Mössbauer process in which the absorption of radiation is accompanied by the absorption and re-emission of a single phonon; there is no net change in the number of phonons, and hence no recoil, but the absorption line is broadened by the finite phonon lifetime.

(*c*) With further increases in the temperature still broader lines corresponding to larger indices m in Eq. 7 become significant, and this signals the onset of multi-phonon absorption and re-emission similar to the single phonon effects in *b*. In practice these may not be resolvable, and what one will see is an apparent broadening of a single anomalous component. This broadening will be approximately linear with temperature, even when γ is assumed to be temperature independent; additional broadening will occur as γ increases with T.

We emphasize that these predictions involve no parameters other than those taken from independent experiments and simulations as quoted above, and that all these predictions are in good agreement with the available data (34–37). Some further analysis of the Mössbauer spectrum is included in Appendix C.

If our analysis of the Mössbauer data in terms of a quasi-harmonic model is correct then careful measurement of the recoil-free fraction $f(T)$ in the neighborhood of $T = \hbar\omega/2k_B \sim 20$ K should detect a small change in slope of ln f vs. T as the breathing mode begins to be excited above its quantum mechanical ground state. The parameters of this slope change should be quantitatively related to the appearance of broad-line components at much higher temperatures, as may be calculated from Eq. 7.

INFRARED AND RAMAN LINESHAPES

Infrared absorption and Raman scattering give a mode-by-mode, rather than atom-by-atom, decomposition of protein dynamics. The lineshapes observed in these spectroscopies are governed in part by the dynamics of vibrational relaxation, and in this section we examine some simple quasi-harmonic models for the relaxation of localized vibrations in the protein interior.

In order for localized internal motions to dissipate their energy to the surrounding solvent they must first transfer this energy to the lower frequency modes of the protein; the long wavelength of the low frequency modes effectively allows for a long-range interaction between the high frequency mode and the solvent. Because of the large difference in frequency between, for example, the carbon monoxide stretching vibration ($\hbar\omega \sim 2{,}000\ cm^{-1}$ [38]) and the breathing modes of the protein, a single phonon excitation of the localized vibrational mode cannot decay into a one-phonon state of the low frequency mode. There must be multi-phonon decay pathways, and this is possible only if there are anharmonic terms in the effective Hamiltonian.

In Appendix D we present some formal results on the anharmonic interactions between high frequency local modes and low frequency breathing modes using a potential surface directly derived from a Morse potential (39) description of the relevant covalent bonds (e.g., Fe–C and C–O in the Mb–CO active site). The essential ideas, however, can be understood from a simple phenomenological analysis. We treat two modes, one at a high frequency Ω and one at a low frequency ω. Neglecting the anharmonic terms the Hamiltonian is

$$H^{(0)} = \frac{1}{2}(P^2 + \Omega^2 Q^2) + \frac{1}{2}(p^2 + \omega^2 q^2), \tag{8}$$

while the lowest order anharmonic terms are

$$H_{\text{anharmonic}} = aq^3 + bq^2Q + cqQ^2 + dQ^3 + \cdots. \tag{9}$$

The first term provides a correction to the properties of the low frequency mode and can be largely taken into account in our definition of ω and the associated relaxation rate γ. Similarly, the last term can be removed by considering the energy levels of the high frequency mode in an anharmonic potential that is still isolated from the rest of the molecule and therefore does not exhibit relaxation. The second and third terms are thus the essential terms for understanding the relaxation process, and both are included in the rigorous analysis of Appendix D. Important qualitative predictions, however, can be obtained by keeping only the term cqQ^2, in which case the Hamiltonian can be rewritten as

$$H = \frac{1}{2}(p^2 + \omega^2 q^2) + \frac{1}{2}(P^2 + (\Omega^2 + 2cq)Q^2), \tag{10}$$

which corresponds to a modulation of the vibrational frequency Ω as the protein breathes.

At the classical level, if the frequency modulation rate (ω) is larger than the relaxation rate of the high frequency vibration[6] then the spectrum of the high frequency mode will split from one line at Ω to a set of lines at $\Omega \pm n\omega$, with $n = 0, 1, 2, \ldots$. This simple pattern of equal spacings survives in a first-order quantum-mechanical analysis of the problem, but is broken by higher-order effects associated with the term *b*. The relative intensities of the sidebands can be calculated reliably only in a quantum-mechanical treatment, and they depend in detail on the anharmonic coupling constants as well as anharmonic coupling to other high-frequency modes (for example, coupling of the C–O stretch to the Fe–C stretch). Some qualitative predictions, however, are independent of the (unknown) details of the potential surface.

[6] If this inequality is not satisfied then the simple picture of the high frequency mode relaxing by irreversible energy transfer to the breathing mode breaks down entirely.

There exists a parameter regime in which the spectrum of the high frequency mode is split into a collection of lines which are spaced approximately by the breathing mode frequency ω. The sidebands are approximately Gaussian as a result of the solvent-induced inhomogeneous broadening of the breathing mode (see above), and their intensities are asymmetric around the dominant band; the dominant band need not be at the bare frequency Ω. As applied to vibrational modes in the active site of myoglobin, our estimate of helix breathing mode properties from above predicts a spectral splitting of $\sim 17\ cm^{-1}$, which is in good agreement with the observed (38) infra-red spectrum of the C–O stretching mode in MbCO.[7]

In other parameter regimes the splitting of the high frequency mode will not be resolvable, and one will observe instead an asymmetric broadening of the vibrational spectrum, as has been detected by Raman scattering for the Fe–His mode (40). If a large number of breathing modes couple to the active site then the splittings of the vibrational spectra are never resolvable and the broadening of the spectral lines becomes symmetric.

The predictions for the C–O stretching spectrum can be tested in greater detail by high-resolution experiments. Each band of the spectrum has a frequency that is determined both by the bare frequency Ω and by corrections related to the breathing frequency ω. Isotopic substitution of the C or O shifts Ω by a simple factor but has no effect (in lowest order) on ω. Rather than having each band center frequency be multiplied by the same isotope-dependent factor, which results in a change of spacing among the bands, we thus predict that the collection of bands will move nearly rigidly (fixed spacing) when the C and O atoms are substituted. The data of Alben et al. (38) are suggestive of such anomalous isotope effects, but the errors quoted in these experiments must be reduced by about one order of magnitude to provide a rigorous test of the theory. At this improved resolution it should also be possible to see an iron isotope effect on ω through its effect on the spacing of the sidebands.[8]

X-RAY DIFFRACTION AND EXAFS

The Debye-Waller factors derived from x-ray diffraction and EXAFS experiments can, in principle, give an atom-by-atom picture of the motions in a protein. Unfortunately, the standard analyses of the diffraction data assume that position of each atom in the protein fluctuates according to an independent Gaussian distribution (41). The distribution of atomic positions $\{q_i\}$ is given (in the classical limit) by the Boltzmann distribution

$$P(\{q_i\}) = Z^{-1} \exp\left[-V(\{q_i\})/k_B T\right].$$

For the rippled potential surfaces assumed in the conformational substates model of Fig. 1 *b* this cannot be a Gaussian distribution. In particular, the use of an anharmonic potential surface to intepret the temperature dependence of the Debye-Waller factors (42) is simply inconsistent, since anharmonicity spoils the Gaussian character of the distribution.

Within the quasi-harmonic approximation the distribution of atomic positions is Gaussian but individual atoms do not move independently, thus spoiling the other key assumption of current Debye-Waller analyses. There are, however, some qualitative questions regarding the magnitude and temperature dependence of the atomic motions that we can study in the quasi-harmonic theory. The displacement of atom μ can be written (as for iron above)

$$\mathbf{x}_\mu = \sum_{\alpha=1}^{N} \mathbf{A}_\alpha(\mu)\tilde{Q}_\alpha,$$

so that the total mean-square displacement is

$$\langle |\mathbf{x}_\mu|^2 \rangle = \sum_{\alpha}^{N} |\mathbf{A}_\alpha(\mu)|^2 \frac{\hbar}{2\omega_\alpha(T)} [2\bar{n}_\alpha(T) + 1].$$

High frequency, localized modes with $\hbar\omega_\alpha(T) \gg k_B T$ contribute a term

$$\langle |\mathbf{x}_\mu|^2 \rangle_{\text{local}} = \sum_{\hbar\omega_\alpha > k_B T} \frac{\hbar |\mathbf{A}_\alpha(\mu)|^2}{2\omega_\alpha(T)},$$

which may be estimated from frequency shifts $\Delta\omega_\alpha$ induced by isotopic mass changes in the μth atom, Δm_μ, using the following argument. When $m_\mu \rightarrow m_\mu + \Delta m_\mu$ the change in the Hamiltonian is

$$\Delta H = \frac{1}{2}\Delta m_\mu \left|\frac{d\mathbf{x}_\mu}{dt}\right|^2$$

$$= \frac{1}{2}\Delta m_\mu \sum_\alpha \sum_\beta [\mathbf{A}_\alpha(\mu) \cdot \mathbf{A}_\beta(\mu)] \frac{d\tilde{Q}_\alpha(t)}{dt}\frac{d\tilde{Q}_\beta(t)}{dt}.$$

To lowest order only terms with $\alpha = \beta$ contribute, and these correspond to frequency shifts:

$$\frac{\Delta\omega_\alpha}{\omega_\alpha} = -\frac{1}{2}\Delta m_\mu |\mathbf{A}_\alpha(\mu)|^2, \tag{11}$$

so that

$$\langle |\mathbf{x}_\mu|^2 \rangle_{\text{local}} = -\sum_{\hbar\omega_\alpha > k_B T} \frac{\hbar}{\omega_\alpha^2} \cdot \frac{\Delta\omega_\alpha}{\Delta m_\mu}. \tag{12}$$

Three modes (at 220 cm^{-1} [43], 304 cm^{-1} [43], and 501 cm^{-1} [44]) in free myoglobin have been observed by Raman spectroscopy to change frequency on isotopic substitution of the iron atom by $\sim 1\ cm^{-1}$/a.m.u.; together

[7] In fact we should observe this splitting in both the ligand bound state and the state reached by flash photolysis, which we term $(Mb \cdots CO)^*_{S-2}$ below. The reason is that the CO motion remains strongly coupled to the protein in this "dissociated" state, as judged by the fact that the Fe–C bond length fluctuations measured in EXAFS (60) do not increase significantly upon photodissociation.

[8] We can calculate the magnitude of this shift in perturbation theory using the $\mathbf{A}_\alpha$(Fe) from the Mössbauer analysis to relate the added mass on the iron to an effective added mass on the breathing mode (see below). The predicted shifts are $\sim 0.1\ cm^{-1}$.

these three local modes determine a root-mean-square displacement of $\delta x_{Fe} \sim 0.003$ nm, which is extremely small in comparison with the estimates obtained from the Debye-Waller factors (45). On the other hand, the low-frequency breathing mode discussed in connection with the Mössbauer data contributes $\delta x_{Fe} \sim 0.03$ nm at 300 K.

Taking the iron atom as an example, high-frequency local modes contribute only a very small amount to the random motions of atoms in the interior of the protein. The bulk of the random motion is governed by the low-frequency breathing modes, in agreement with molecular dynamics simulations (2), and these modes must also carry nearly all of the temperature dependence that the motion exhibits. Atoms with large motions have these large motions by virtue of strong coupling to the low frequency modes.

A second qualitative prediction is that the large motions of atoms in the interior of the protein would appear to be much smaller (approximately by an order of magnitude in the case of the Fe atom) and less strongly temperature dependent if we look only at the local vibrations of each atom relative to its near neighbors. It is precisely this sort of motion which determines the Debye-Waller factors in EXAFS experiments, and indeed the EXAFS spectrum of the iron atom in heme proteins (46) exhibits small, nearly temperature-independent Debye-Waller factors.[9] This difference between local and collective motions does not have a natural interpretation in terms of the conformational substates model of Fig. 1 *b*. More quantitative tests of the quasi-harmonic model could be made by comparing the EXAFS measurement of atomic motion to the frequency shifts observed in the vibrational spectrum of Mb upon combined isotopic substitution of the iron atom and its near neighbors, using a generalization of Eq. 12 above.

REACTION RATES IN A QUASI-HARMONIC PROTEIN

The rebinding of CO to myoglobin following flash photolysis occurs by a sequence of reactions, of which only one is observed at temperatures below 160 K (5). This last transition is accompanied by a change in spin state of the heme iron (47, 48), and hence involves at least two electronic states. We refer to the liganded low spin state as $(\mathrm{Mb} \cdot \mathrm{CO})_{S=0}$ and to the dissociated high spin state reached by flash photolysis as $(\mathrm{Mb} \cdot \cdot \cdot \mathrm{CO})^*_{S=2}$. In each of these electronic states we can construct a quasi-harmonic description of the molecule parameterized by the quasi-normal mode frequencies, transformation coefficients from quasi-normal coordinates to atomic coordinates, and the equilibrium positions of each quasi-normal coordinate. In addition there is an overall energy difference ϵ between the two electronic states (binding energy) and a matrix element V that connects the two states; we approximate this matrix element as a coordinate-independent constant (the Condon approximation). The calculation of transition rates in such coupled electron-phonon systems has been discussed by several groups (20, 49–53); we follow reference 20 and as a first approximation neglect vibrational frequency shifts between the two electronic states, concentrating instead on the structural changes that accompany the reaction.

Within the approximations of reference 20, which are justified for the myoglobin problem in Appendix E, the reaction rate for $(\mathrm{Mb} \cdot \cdot \cdot \mathrm{CO})^*_{S=2} \rightarrow (\mathrm{Mb} \cdot \mathrm{CO})_{S=0}$ may be written as

$$k = V^2 \int d\Omega_1 \int d\Omega_2 \cdot \cdot \cdot \int d\Omega_N \delta(\epsilon/\hbar - \Omega_1 - \Omega_2 - \cdot \cdot \cdot - \Omega_N) G_1(\Omega_1) G_2(\Omega_2) \cdot \cdot \cdot G_N(\Omega_N), \quad (13)$$

where the spectral function of each mode $G_\alpha(\Omega)$ is of the same form as $F_\alpha(\Omega)$ in Eq. 10, albeit with different coupling constants S_α. As for the Mössbauer spectra, high frequency modes need not be treated explicitly but can be absorbed into a redefinition of the parameters (54); for the present problem the situation is even simpler since the relevant high frequency modes are apparently weakly coupled, as described in Appendix E. Finally, as in all of the analysis above, we concentrate on a single low-frequency vibrational mode, tentatively identified with stretching or bending of the F alpha helix.

The single mode model is sketched in Fig. 2. From this picture we can think of the reaction as occurring in two

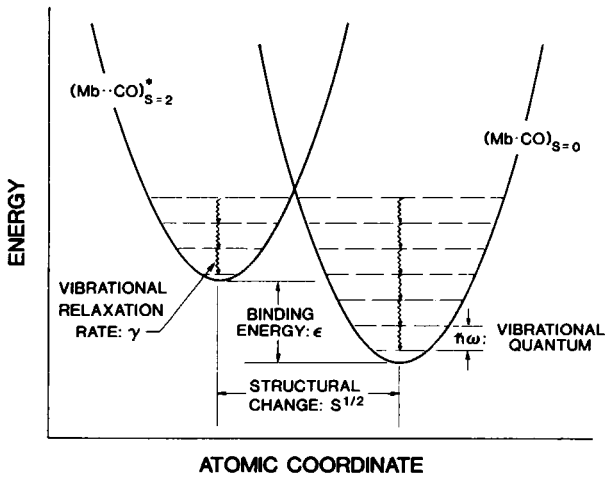

FIGURE 2. Simple model of CO binding to myoglobin. Two electronic states are identified as reactants and products, and the structural changes upon ligand binding are summarized by displacement along a single quasi-normal coordinate. Interactions with the solvent damp the vibrational motion of this coordinate and lead to a distribution of its vibrational frequency.

[9]The problems in the interpretation of Debye-Waller factors are much less severe for EXAFS than they are for x-ray diffraction, since in diffraction experiments one is sensitive to all possible correlations among motions of different atoms, while in EXAFS the only relevant correlations are among the relative motions of a few atoms in the first coordination shells. These motions are often nearly orthogonal, so that their correlations cannot contribute to the observed absorption intensities.

stages. First, a molecule in the nth vibrational state of the dissociated species, state $|n; (\mathrm{Mb} \cdot \cdot \cdot \mathrm{CO})^*_{S-2}\rangle$, makes a transition to the n' vibrational state of the ligand-bound species, $|n'; (\mathrm{Mb} \cdot \mathrm{CO})_{S-0}\rangle$. Second, the molecule vibrationally relaxes to states $|n''; (\mathrm{Mb} \cdot \mathrm{CO})_{S-0}\rangle$ with $n'' < n'$. The first transition is a coherent process which conserves energy and is driven by the electronic matrix element V; energy dissipation and irreversibility arise only in the second stage of the transition (for discussion see reference 54).

In this two-stage picture it is clear that the reaction rate will depend on the overlap of the n and n' vibrational levels in the two electronic states (Franck-Condon factors). This leads to an approximately Gaussian variation of the reaction rate with changes in binding energy, and this is the energy gap law (55). Since the vibrational overlap depends on the vibrational frequency, there is a frequency dependence of the reaction rate and this is also approximately Gaussian. In the regime where a low-frequency vibrational mode is strongly coupled to the reaction this effect results in a very strong variation of the reaction rate with small changes in vibrational frequency.

In addition to the energy gap law, energy conservation in the first stage of the transition requires that the states $|n; (\mathrm{Mb} \cdot \cdot \cdot \mathrm{CO})^*_{S-2}\rangle$ and $|n'; (\mathrm{Mb} \cdot \mathrm{CO})_{S-0}\rangle$ be nearly equal in energy. This is only possible if the binding energy ϵ is nearly an integer multiple of the vibrational quantum $\hbar\omega$. We emphasize that this resonance condition is a purely quantum mechanical effect—it has no content in the limit $\hbar \to 0$—but that it can be significant even at temperatures such that $k_B T > \hbar\omega$. The resonance condition is significant whenever the linewidths of the vibrational states are small, that is whenever the vibrational relaxation γ is slow. The quantum resonances result in a very sensitive dependence of the reaction rate on the vibrational frequency ω, although this is significant only in small ranges of frequency surrounding the resonant peaks.

The prediction of large variations in reaction rate with small changes in protein vibrational frequency—whether these arise from the energy gap law or from quantum resonances—provides a clear and nontrivial example of how picosecond ($2\pi/\omega \approx 1.5 \times 10^{-12}$ s) molecular dynamics can influence the functional behavior of a protein on the biochemical time scale. Further, since protein molecules in solution have a distribution of vibrational frequencies (see above), the sensitive dependence of reaction rate on frequency will generate a broad distribution of reaction rates even if the distribution of frequencies is fairly narrow. Specifically, in frozen solution each molecule is stuck with a particular frequency ω and hence a particular reaction rate $k(\omega)$, so we will observe an overall reaction time course

$$N(t) = \int d\omega P(\omega) e^{-k(\omega)t}, \tag{14}$$

where $P(\omega)$ is the probability of having frequency ω. This time course is clearly nonexponential and thus may provide an explanation for the observed (5) nonexponential kinetics of CO rebinding to myoglobin. The critical point is that the quasi-harmonic approximation provides a framework for explicitly calculating $k(\omega)$, and this allows us to relate our description of the kinetics to the analysis of spectroscopic data given above.

To calculate the time course of the reaction we need values for six parameters. The first two are the vibrational frequency and relaxation time, which have been discussed in detail. Next is the binding energy ϵ, which is known from kinetic experiments (5). The fourth parameter is the electronic matrix element V, which sets an overall time scale for the reaction but does not contribute to either the temperature dependence or the nonexponential structure of the reaction time course.

The fifth parameter is the structural change upon ligand binding, measured by the dimensionless coupling constant S. With the other parameters held fixed, the reaction rate and particularly its temperature dependence are extremely sensitive to S, and available data on the structure of reactants and products do not lead to an estimate that is sufficiently precise to overcome this sensitivity. Qualitatively, however, a coupling S corresponds to a motion of the F helix by $\delta x \sim 2(\hbar S/2m\omega)^{1/2}$ where m is the helix mass calculated above. Very large coupling constants, $S \sim 50$, are therefore consistent with the rather small $\delta x \sim 0.05$ nm motions of the F helix observed crystallographically upon ligand binding (27). Even larger effective coupling constants may be relevant since we have approximated the total structural change upon ligand binding by motion along a single quasi-normal coordinate.[10]

Finally, in order to calculate the reaction time course from Eq. 14 we must have an expression for the inhomogeneous lineshape $P(\omega)$. As discussed above, this lineshape is typically Gaussian, with standard deviation $\Delta\omega$, and can in principle be measured in Raman or infrared spectra. We expect that $\Delta\omega$ will be small in comparison with ω, and $\Delta\omega \sim 1$ cm^{-1} is reasonable.

With these parameter estimates we are ready to compare the data of reference 5 to the theoretical predictions from Eq. 14. The numerical details of the computations are given in Appendix E, and the results are shown in Fig. 3 with final parameter values in the legend. The agreement between theory and experiment is quite good. We emphasize that the vibrational frequency and relaxation rate were taken as known from the analyses above, as was the binding energy, so that the only important free parameters

[10]Finally, our use of the Condon approximation means that we ignore the possibility of electron-phonon coupling in the matrix element itself; this adds further uncertainty to our interpretation of the one remaining electron-phonon coupling constant S. We conclude that S is, at the present level of description, a phenomenological parameter that may be qualitatively but not quantitatively estimated by comparison with the available structural data.

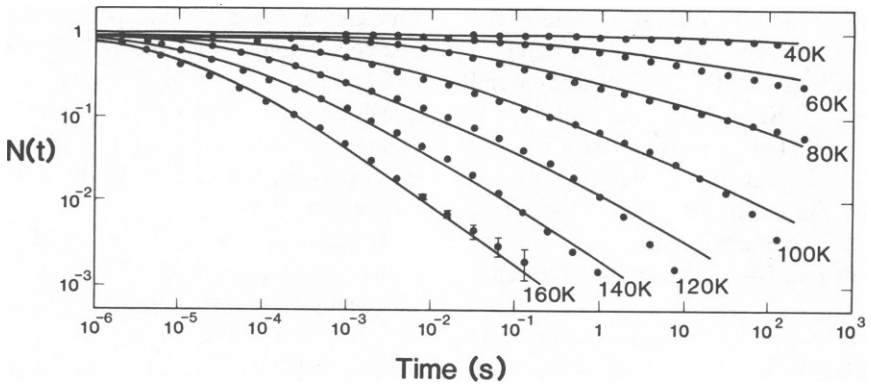

FIGURE 3. Time course of CO rebinding to myoglobin, calculated as described in the text (solid lines) and compared with the data of reference 5 at several temperatures. Parameters are the binding energy $\epsilon = 0.9$ eV, the vibrational frequency $\hbar\omega = 20$ cm^{-1}, the vibrational linewidth $\hbar\gamma = 0.01$ cm^{-1}, the dimensionless coupling constant $S = 170$, the inhomogeneous vibrational linewidth $\hbar\Delta\omega = 1.6$ cm^{-1}, and the electronic matrix element $V = 1.1$ cm^{-1}. As discussed in the text, most of these parameters were determined from independent analyses of spectroscopic data, and only two are actually required for fitting of the temperature dependent nonexponential decays shown here.

were S and $\Delta\omega$; even for these quantities our rough estimates are very close to the final results.

DISCUSSION

The arguments given here demonstrate that the quasi-harmonic approximation provides a framework within which a large body of data can be understood at least semi-quantitatively. Most remarkably, the essential observations on ligand binding in myoglobin—the anomalous low-temperature kinetics, the broad-line components of the Mössbauer spectrum, the magnitude and temperature dependence of atomic motions detected by x-ray diffraction and EXAFS, and the splitting of the CO stretching spectrum—can all be understood in terms of the simplest possible quasi-harmonic theory, in which we explicitly include only one low frequency narrow linewidth breathing mode of the protein.

All of the data discussed here have previously been interpreted in terms of the conformational substates model of protein dynamics (4), which envisions the potential surface of the protein to be as in Fig. 1 *b*. Specifically, the non-exponential rebinding kinetics have been attributed (5) to each molecule being trapped (at low temperature) in a different substate, with different substates being assigned different reaction rates; the broad-line Mössbauer spectrum has been associated with hopping among substates (34), which may approximate over-damped motion on a smooth potential surface (36, 37); and the splitting of the CO stretch is explained by assigning different substates different vibrational frequencies (38).

Although both the substates and the quasi-harmonic models account for the same experiments, they convey radically different pictures of protein dynamics: protein motion in the substates picture consists of over-damped, diffusive 'hopping' among conformations whereas in the quasi-harmonic theory we envision smooth vibrational motion that can store kinetic energy over time scales as long as a nanosecond. Perhaps surprisingly, none of the existing data on myoglobin directly determines whether the functionally important protein motions are under-damped or over-damped. This is clearest for the Mössbauer experiment: *if* the motion is over-damped then the width of the broad line determines the diffusion constant for hopping among conformations, while *if* the motion is under-damped this width is simply the vibrational linewidth.

We emphasize that our analysis of myoglobin dynamics in terms of a quasi-harmonic theory does not preclude the existence of some conformational substates, such as those associated with tyrosine ring flips and rotation of surface residues. Indeed one might identify the different solvent shell configurations that we discuss with the conformational substates originally proposed by Austin et al. (5) to account for nonexponential kinetics at low temperatures. The critical point, however, is that in the quasi-harmonic theory transitions among these "solvent substates" do not contribute to the functionally interesting dynamics of the molecule, the dynamics that controls chemical reaction rates. Further, transitions among substates are not identified with any of the unusual spectroscopic results that are found for myoglobin since we claim that these spectroscopies probe dynamical degrees of freedom which *are* relevant to the determination of reaction rates. In effect the substates that do exist in our description provide only a background against which the functionally important dynamics proceed, and it is these dynamics that we describe by a quasi-harmonic model.

It has been suggested (2–4) that molecular dynamics simulations provide evidence for liquid-like behavior in the interior of a protein, with the result that motions are over-damped and diffusive as postulated in the substates model. In practice, the results of molecular dynamics simulations are summarized as correlation functions for local fluctuations, for example in bond angle. In the

quasi-harmonic model these local quantities are superpositions of many quasi-normal coordinates with, in general, widely varying frequencies. As time proceeds the oscillations in different modes run out of phase with one another, resulting in an apparent loss of correlations long before any single mode has lost any energy. The correlation times for local motions therefore have nothing to do with the vibrational linewidth and the question of over-damped vs. under-damped motion is not addressed. Indeed if one looks at a simple perfect crystal, the correlation time for local motions will typically be the inverse of the Debye frequency (30), on the order of 10^{-13} s, while obviously some sound waves in the crystal propagate unattenuated over macroscopic distances.

The question of under-damped vs. over-damped motion can only be decided by direct experiment, and we have seen that experiments on model systems support both the qualitative idea of under-damped motion and the quantitative value of the vibrational lifetime required to account for the myoglobin data in a quasi-harmonic theory. Ideally the predictions of the quasi-harmonic theory should be tested by analogous experiments on myoglobin itself, but these will be quite difficult. Our estimate of phonon lifetimes in the nanosecond range implies, however, that it should be possible to observe unrelaxed fluorescence, fluorescence in which the emission spectrum depends on excitation wavelength and on the time since excitation;[11] this may already have been observed (56).

In comparing the quasi-harmonic and substates approaches it should be pointed out that the latter model fails in several instances to give a consistent quantitative account of the data. First, as discussed elsewhere (57), the estimates of barrier heights and structural changes between substates may be difficult to reconcile with the known properties of molecular potential energy surfaces without having tunneling among the substates at rates too large to be consistent with the interpretation of the kinetic data in terms of a stationary distribution over substates at low temperatures. This difficulty may be resolved in the more complex hierarchical version of the substates model (58), but this approach needs to be better developed before it can give quantitative predictions.

Second, analysis of the low-temperature kinetics in terms of the substates model led to the prediction (59) that the Fe–C bond length should change by $\Delta x_{Fe\text{-}C} \sim 0.05$ nm upon ligand binding, and that this bond length change should have a broad distribution, $\delta x \sim 0.01$ nm, reflecting rebinding from different substates. Since molecules with different Fe–C bond lengths react at different rates, one would expect to see a gradual shift in the bond length distribution during the rebinding reaction. While some of the predictions might change in more complex versions of the substates model, none of them have been confirmed by EXAFS measurements of the Fe–C bond length in the photolyzed state (60), although to be fair the last (dynamic) prediction is not tested by the available data.

In particular, the observed bond length changes are an order of magnitude smaller than the substates predictions (which has enormous consequences for the reaction rate, where the magnitude of the structural change enters exponentially!) and the variance in bond lengths has the small value expected from the quasi-harmonic analysis (see above) rather than the large value predicted by the substates model. In view of these small displacements, the existing interpretation of the kinetic isotope effects (59) also fails, and alternative interpretations in terms of the quasi-harmonic theory are discussed in Appendix F. Clearly it is of great importance to repeat the EXAFS experiment,[12] perhaps on isolated β hemoglobin chains in which the rebinding reaction proceeds with a reasonable rate even at very low temperatures (5).

In addition to experiments that discriminate between the substates and quasi-harmonic theories, there are many experiments which can provide detailed tests of the quasi-harmonic predictions; several of these have been discussed where appropriate in the main text and in the Appendices. Perhaps the most direct test would be to observe the strong dependence of reaction rate on vibrational frequency which is predicted by the theory. In the infrared spectrum of the C-O stretch, for example, we predict that the splitting among lines is related to the frequency of the F helix breathing mode, so that molecules with slightly different splittings are reacting at different rates. The average splitting of the bands should therefore be time dependent during the recombination reaction, and preliminary calculations suggest that the changes in splitting are on the order of 1 cm^{-1}.

The fact that the quasi-harmonic theory leads to definite quantitative predictions reinforces the conclusion that it provides an attractive framework within which to think about protein dynamics. The fact that we can account for such a large body of data with a small number of parameters, each of which can be directly compared with more than one piece of data, certainly indicates that our picture is simpler and more tightly constrained than the substates model. Finally, in more detailed versions of the quasi-harmonic theory there is the hope that with sufficient spectroscopic data it will actually be possible to do a parameter-free calculation of the reaction rate, its temperature dependence, and the inhomogeneity which leads to nonexponential decays.

[11]We recall that typical fluorescence lifetimes are in the range of several nanoseconds, which is usually sufficient for the molecule to vibrationally relax into an equilibrium distribution within the electronic excited state reached by photon absorption. This situation leads to relaxed fluorescence, which has no memory of the excitation, in contrast to the unrelaxed fluorescence predicted here.

[12]While we cannot make a precise prediction for $\Delta x_{Fe\text{-}C}$ from our analysis of the kinetic data, the simple arguments of Appendix E suggest $\Delta x_{Fe\text{-}C} \leq 0.004$ nm.

APPENDIX A

Foundations of the Quasi-Harmonic Approximation

We begin by collecting the basic formulae and notation used in our calculations. We have a set of quasi-normal coordinates $\tilde{Q}_\alpha$ associated with phonon frequencies $\omega_\alpha(T)$, where we explicitly indicate that the mode frequencies can depend on temperature. To describe the modes quantum-mechanically we introduce operators $\hat{Q}_\alpha$ and $\hat{P}_\alpha$ corresponding to the coordinate $\tilde{Q}_\alpha$ and its conjugate momentum $\tilde{P}_\alpha$, respectively. The effective Hamiltonian (see below and Appendix B) is of the form

$$\mathbf{H} = \frac{1}{2}\sum_\alpha [\hat{P}_\alpha^2 + \omega_\alpha^2 \hat{Q}_\alpha^2] + \text{anharmonic corrections} + \text{damping}, \quad \text{(A1)}$$

where "anharmonic corrections" represent the terms responsible for phonon-phonon interactions and "damping" represents those terms responsible for coupling the coordinates $\tilde{Q}_\alpha$ to a heat bath and generating the vibrational relaxation rates γ_α. In the absence of these extra terms, the dynamics of the system are completely described by the correlation functions

$$\langle \hat{Q}_\alpha(t)\hat{Q}_\beta(t')\rangle = \delta_{\alpha\beta}\frac{\hbar}{2\omega_\alpha(T)}[2\bar{n}_\alpha(T)+1]\cos[\omega_\alpha(t-t')] + i\delta_{\alpha\beta}\frac{\hbar}{2\omega_\alpha(T)}\sin[\omega_\alpha(t-t')], \quad \text{(A2)}$$

where the average number of phonons

$$\bar{n}_\alpha(T) = \frac{1}{e^{\hbar\omega_\alpha(T)/k_BT}-1}, \quad \text{(A3)}$$

and all higher order correlation functions (averages of products of three or more operators) can be factored into these elementary correlations (14–18). We may describe damping by rigorous solution of models such as that discussed in Appendix B (61, 62), but for all the quantities of interest here it is a good approximation simply to replace the factor $\exp\{\pm i\omega_\alpha(t-t')\}$ in the correlation functions by $\exp\{\pm i\omega_\alpha(t-t') - \gamma_\alpha|t-t'|\}$. Anharmonic corrections will be discussed as needed.

The validity of the quasi-harmonic approximation can only be assessed by comparison with real experiments or carefully constructed computer simulations. Nonetheless it is important to understand how one could construct the quasi-harmonic approximation from a real potential surface, both for a good physical picture of the quasi-normal modes and so that if desired these modes could be found by explicit computation.

We describe the molecule in terms of classical mechanics; a quantum version of these arguments is straightforward. Each coordinate of the molecule obeys the equation of motion

$$\frac{d^2q_\alpha(t)}{dt^2} = -\frac{\partial V(\{q_\alpha(t)\})}{\partial q_\alpha(t)}. \quad \text{(A4)}$$

We are interested in correlation functions such as $\langle q_\alpha(t)q_\beta(t')\rangle$, which then obeys

$$\frac{d^2\langle q_\alpha(t)q_\beta(t')\rangle}{dt^2} = -\left\langle \frac{\partial V(\{q_\alpha(t)\})}{\partial q_\alpha(t)} q_\beta(t')\right\rangle, \quad \text{(A5)}$$

where $\langle\cdots\rangle$ denotes an average over either a long time period or many samples of a short time period. The spirit of the quasi-harmonic approximation is to replace these exact averages by averages over a distribution of coordinates that is of the same form as that obtained from a harmonic system, i.e. the probability of the system having the set of coordinates $\{q_\alpha(t)\}$ is a Gaussian function of the q_α. Because of this Gaussian property averages of very complicated polynomial functions of q_α can be broken up into sums of products of the elementary averages, and the relevant elementary averages are just $\langle q_\alpha(t)q_\beta(t')\rangle$. Note that this Gaussian distribution has as parameters the N equilibrium positions of each coordinate and the N^2 "spring constants" that determine the correlation matrix for the total fluctuations $\langle q_\alpha(t)q_\beta(t)\rangle$.

Carrying out the averaging for the right hand side of Eq. A5, we decompose the full average into elementary averages, as noted above. The first such term is one in which averaging over all factors of q_α in the potential are independent of the extra q_β required to determine the correlation function; this first term is then

$$\left\langle \frac{\partial V(\{q_\alpha\})}{\partial q_\alpha(t)} q_\beta(t')\right\rangle^{(1)} = \left\langle \frac{\partial V(\{q_\alpha\})}{\partial q_\alpha(t)}\right\rangle \langle q_\beta(t')\rangle. \quad \text{(A6)}$$

This term can be eliminated if we choose the distribution so that $\langle \partial V(\{q_\alpha\})/\partial q_\alpha\rangle = 0$, which corresponds to an ensemble in which there is no average force on any atom. This constraint gives us N conditions on the distribution function, and essentially these conditions determine the equilibrium positions of all the atoms.

At the next level of approximation we consider terms in which $q_\beta(t')$ of Eq. A5 is paired with one factor of $q_\gamma(t)$ pulled out of the potential V, and successive approximations are obtained by iteration. The result, making use of the constraint $\langle \partial V(\{q_\alpha\})/\partial q_\alpha\rangle = 0$, is

$$\frac{d^2\langle q_\alpha(t)q_\beta(t')\rangle}{dt^2} = -\sum_\gamma \left\langle \frac{\partial^2 V(\{q_\alpha(t)\})}{\partial q_\alpha(t)\partial q_\gamma(t)}\right\rangle \times \langle q_\gamma(t)q_\beta(t')\rangle + \ldots, \quad \text{(A7)}$$

where the average is over the approximate quasi-harmonic probability distribution function. Eq. A7 approximates the equations of motion for the correlation functions of a harmonic system with potential surface

$$V_H(\{q_\alpha\}) = \frac{1}{2}\sum_{\alpha\beta} q_\alpha \left\langle \frac{\partial^2 V(\{q_\alpha\})}{\partial q_\alpha \partial q_\beta}\right\rangle q_\beta. \quad \text{(A8)}$$

To be self-consistent, we must have chosen our quasi-harmonic distribution as the equilibrium distribution on this potential surface, and this determines the N^2 "spring constants."

In fact we can systematically improve on this self-consistent version of the quasi-harmonic approximation. By keeping further terms in the expansion of Eq. A7 we can show that the self-consistent quasi-normal modes interact through an effective anharmonic potential surface of the form

$$V_{\text{int}}^{\text{eff}}(\{q_\alpha\}) = \frac{1}{3!}\sum_{\alpha\beta\gamma}\left\langle \frac{\partial^3 V(\{q_\alpha\})}{\partial q_\alpha \partial q_\beta \partial q_\gamma}\right\rangle^{(0)} q_\alpha q_\beta q_\gamma + \frac{1}{4!}\sum_{\alpha\beta\gamma\delta}\left\langle \frac{\partial^4 V(\{q_\alpha\})}{\partial q_\alpha \partial q_\beta \partial q_\gamma \partial q_\delta}\right\rangle^{(0)} q_\alpha q_\beta q_\gamma q_\delta + \cdots, \quad \text{(A9)}$$

where we explicitly indicate that all averages are carried out with the zero-order self-consistent distribution. These anharmonic terms can be used, in perturbation theory, to compute corrections to the self-consistent quasi-normal vibrational frequencies and mode structures. In addition they contribute to vibrational relaxation processes in which energy in one mode becomes shared among many. These perturbative calculations are discussed in standard texts (14–18).

To summarize, the classical quasi-harmonic approximation consists of a Gaussian approximation to the distribution of atomic positions. The average positions are determined by the requirement that there be no average force on each atom, while the fluctuations in position are determined by the average spring constants defined in the potential V_H. The validity of the harmonic approximation requires that the spring constants determined near the minimum of the potential surface are good approximations to the curvature of the potential surface at any time

during its evolution. Clearly the quasi-harmonic approximation rests on a much less stringent assumption, namely that the curvature of the potential surface at each instant of time is close to the average curvature experienced during the whole evolution. Even if the spring constants determined near the position of minimum potential energy are very different from the average spring constants, the self-consistent Gaussian distribution may thus still provide an excellent approximation to the exact distribution of atomic positions, and it is for this reason that the quasi-harmonic approximation can be effective even when the harmonic approximation is not.

APPENDIX B

From Solvent to Heat Bath

We consider a protein molecule, with internal coordinates q_α moving on a potential surface $V(\{q_\alpha\})$, to be sitting in an essentially infinite bath of solvent. Imagine that we hold the internal coordinates fixed, but allow the solvent to evolve dynamically; for the present we consider this evolution to be classical (Newton's equations), but the generalization to quantum dynamics is straightforward. As the solvent evolves it will apply forces $F_\alpha(t)$ to each internal coordinate of the protein. This force will have some time-average value

$$\langle F_\alpha \rangle = \lim_{T\to\infty} \frac{1}{T} \int_0^T dt F_\alpha(t), \tag{B1}$$

and it will also exhibit fluctuations $\delta F_\alpha(t)$. If the force on any one coordinate results, directly or indirectly, from a large number of solvent molecules (and there is strong evidence of this even in simple systems [26]), then by the central limit theorem $\delta F_\alpha(t)$ is a Gaussian stochastic process, completely described by the set of correlation functions $C_{\alpha\beta}(t - t') = \langle \delta F_\alpha(t)\delta F_\beta(t') \rangle$, or equivalently by the spectral densities

$$S_{\alpha\beta}(\Omega) = \int_{-\infty}^{\infty} d\tau e^{+i\Omega\tau} \langle \delta F_\alpha(t)\delta F_\beta(t-\tau) \rangle. \tag{B2}$$

To be general we must allow these forces to depend on the protein coordinates, so we write $\langle F_\alpha(\{q_\alpha\}) \rangle$ and $S_{\alpha\beta}(\Omega; \{q_\alpha\})$.

The evolution of the solvent that we have been considering is presumably taking place in equilibrium at some temperature T. Because of the fluctuation-dissipation theorem (63) we know that any two systems that give the same fluctuations in thermal equilibrium must also exhibit the same dynamics. Thus if we make a model of the solvent that has the appropriate force spectra $S_{\alpha\beta}(\Omega; \{q_\alpha\})$ then this model will mimic all features of solvent dynamics that are relevant for its interaction with the protein. This is a nontrivial conclusion, since it implies that all the dynamics of protein-solvent interactions can be derived from independent simulations of protein and solvent evolution.

Following the Caldeira-Leggett (61) analysis of models for heat baths we consider the Hamiltonian

$$H = \sum_\alpha \frac{p_\alpha^2}{2m_\alpha} + V(\{q_\alpha\}) + V_s(\{q_\alpha\}) + \frac{1}{2} \sum_{i\gamma} \{p_{i\gamma}^2 + \omega_i^2[x_{i\gamma} - \phi_{i\gamma}(\{q_\alpha\})]^2\}, \tag{B3}$$

where p_α is the momentum and m_α is the mass associated with coordinate q_α, the $\{p_{i\gamma}, x_{i\gamma}\}$ are a set of heat bath coordinates and momenta, and $V_s(\{q_\alpha\})$ is the change in the potential surface of the protein atoms alone upon solvation. Corresponding to the situation described above, we consider the dynamics of the $\{x_{i\gamma}\}$ with the $\{q_\alpha\}$ fixed. Newton's equations become

$$\frac{d^2x_{i\gamma}}{dt^2} = -\frac{\partial H}{\partial x_{i\gamma}} = -\omega_i^2[x_{i\gamma} - \phi_{i\gamma}(\{q_\alpha\})], \tag{B4}$$

which is just the equation for a simple harmonic oscillator of unit mass, frequency ω_i, and equilibrium position $\phi_{i\gamma}(\{q_\alpha\})$. At temperature T such a system exhibits Gaussian fluctuations in $x_{i\gamma}$, with a correlation function

$$\langle \delta x_{i\gamma}(t)\delta x_{i\gamma}(t') \rangle = \frac{k_B T}{\omega_i^2} \cos[\omega_i(t - t')]. \tag{B5}$$

On the other hand, the force acting on coordinate q_α is given by

$$F_\alpha = -\frac{\partial H}{\partial q_\alpha} = -\frac{\partial V_s(\{q_\alpha\})}{\partial q_\alpha} + \sum_{i\gamma} \omega_i^2 \frac{\partial \phi_{i\gamma}}{\partial q_\alpha} [\phi_{i\gamma}(\{q_\alpha\}) - x_{i\gamma}]. \tag{B6}$$

With the identification of the $x_{i\gamma}$ as harmonic oscillator coordinates the average force becomes

$$\langle F_\alpha(\{q_\alpha\}) \rangle = -\frac{\partial V_s(\{q_\alpha\})}{\partial q_\alpha}, \tag{B7}$$

and the spectral functions are

$$S_{\alpha\beta}(\Omega; \{q_\alpha\}) = \frac{1}{2} k_B T \sum_{i\gamma} \omega_i^2 \frac{\partial \phi_{i\gamma}}{\partial q_\alpha} \frac{\partial \phi_{i\gamma}}{\partial q_\beta} 2\pi\delta(|\Omega| - \omega_i). \tag{B8}$$

If we imagine that the heat bath is infinitely large then we can replace all sums over discrete variables $x_{i\gamma}$ by integrations over a continuous set of variables $x_\gamma(z)$, where z is a continuous parameter that we may choose (without loss of generality) to be the frequency of the mode. Then $\phi_{i\gamma}(\{q_\alpha\}) \to \phi_\gamma(\omega; \{q_\alpha\})$ and

$$S_{\alpha\beta}(\Omega; \{q_\alpha\}) \to \frac{1}{2} k_B T \Omega^2 \sum_\gamma \frac{\partial \phi_\gamma(|\Omega|; \{q_\alpha\})}{\partial q_\alpha} \frac{\partial \phi_\gamma(|\Omega|; \{q_\alpha\})}{\partial q_\beta}. \tag{B9}$$

In effect the correlation matrix $S_{\alpha\beta}$ is just proportional to the square of the "coupling matrix" $g_{\alpha\gamma} = \partial\phi_\gamma/\partial q_\alpha$, and since $S_{\alpha\beta}$ is positive[13] it is always possible to find some $g_{\alpha\gamma}$ which will simulate the fluctuating forces applied by the solvent.[14] This completes the proof that the Caldeira-Leggett Hamiltonian can be made equivalent to the protein/solvent interaction problem for appropriate choices of parameters. In fact the message of the Caldeira-Leggett (61) analysis is that any reasonable model of a heat bath can be mapped to the harmonic oscillator Hamiltonian, so we have really shown that the dynamics of protein/solvent interactions are equivalent to protein/heat bath interactions, as promised.

If the functions $\phi_{i\gamma}$ are linear in the coordinates $\{q_\alpha\}$ then the Hamiltonian of Eq. B3 describes linear, possibly frequency dependent damping of the protein motion by the solvent. The frequency dependent damping constants can be written in terms of the spectral densities $S_{\alpha\beta}$ and only these spectral densities; there are no hidden arbitrary parameters. Quadratic terms in the dependence of $\phi_{i\gamma}$ on $\{q_\alpha\}$ give rise to dephasing of the vibrations and, if they involve coupling to very low-frequency ($\omega_l \to 0$) solvent modes, inhomogeneous broadening of the protein vibrations.

APPENDIX C

Acoustic Modes and the Recoiless Fraction

As a first approximation we describe the acoustic modes of a myoglobin crystal by the isotropic Debye model, for which the attenuation of the

[13] Also, in a classical system such as we have been discussing, the spectral density is an even function of frequency, so there is no difficulty associated with the absolute value signs in these equations. The quantum case requires a bit more care, but there is still no real difficulty with positive vs. negative frequencies.

[14] Indeed it is clear that there may be many such models, all of which will generate equivalent dynamics.

Mössbauer spectrum is calculated in standard texts (30):

$$A_{\text{Debye}}(\theta, T) = \exp\left\{-\frac{k^2\hbar v_c}{12\pi^2 Ms}\left(\frac{k_B T}{\hbar s}\right)^2 \times \int_0^{\theta/T} dx\, x \coth x\right\}, \quad \text{(C1)}$$

where s is the speed of sound in the crystal, v_c is the volume of a unit cell, and M is the molecular mass contained in this unit cell; these parameters determine the Debye temperature $\Theta = (\hbar s/k_B)(6\pi^2/v_c)^{1/3}$. The parameters M and v_c are known from the crystal structure of myoglobin (45) and since the crystal is largely water we take $s \sim 10^3$ m/s. The result is a very low Debye temperature, $\Theta = 7.4$ K, and for temperatures $T \gg \Theta$ we find

$$A_{\text{Debye}}(\theta, T) \approx \exp\left(-\frac{T}{140\text{ K}}\right), \quad \text{(C2)}$$

or, defining an effective mean-square displacement of the iron atom through $\ln A(T) = -(1/6)k^2\langle(\delta x_{Fe})^2\rangle$,

$$\langle(\delta x_{Fe})^2\rangle_{\text{Debye}} \approx (0.04\text{ nm})^2\left(\frac{T}{300\text{ K}}\right). \quad \text{(C3)}$$

Comparing with the experimental values of $\langle(\delta x_{Fe})^2\rangle$ (34, 35; our definition of the variance differs from these references by a factor of 3) one sees that acoustic phonons could very well be the dominant factor in determining the magnitude of the recoiless fraction.

In regard to the temperature dependence of the acoustic phonon contribution, it should be remembered that the protein—and presumably the protein crystal—melts at $T_c \sim 350$ K. Simple theories of crystal melting (64) predict that the mean-square displacement acquires an extra temperature dependence $\sim (1 - T/T_c)^{-1}$, so that at 300 K we expect $\langle(\delta x_{Fe})^2\rangle$ to be a factor of seven larger than would be estimated by linear extrapolation from low temperatures. This is in good agreement with experiment (34, 35, 37). Similar melting considerations apply to the protein breathing mode discussed in the text, and this is important for a quantitative description of the temperature-dependent relative intensities of narrow and broad line components in the spectrum.

Previous discussions of motion in protein crystals have assumed that contributions from the lattice as a whole are dominated by static translational disorder, while the estimates given here demonstrate that dynamic disorder contributed by acoustic phonons is probably significant. Such a contribution, which is necessarily temperature dependent, implies that corrections for lattice disorder may be misleading; in particular acoustic modes contribute to apparent motion in both Mössbauer and crystallographic experiments, so attempts to separate lattice effects by comparison of the two techniques are not valid.

More quantitative discussions could be given if the sound velocity in myoglobin crystals were measured directly, ideally along all the crystal axes, or if the acoustic modes could be detected by inelastic neutron scattering. The Debye temperature is measurable in low temperature specific heat experiments, although these should be done on $(\text{Mb} \cdot \text{CO})_{S=0}$ to avoid the complications of spin degrees of freedom.

APPENDIX D

Rigorous Results for Vibrational Lineshapes

Consider a small molecule AB imbedded in a protein. We will think of atom A as a part of the protein and of atom B being as being covalently bonded to A through a Morse potential (39); obviously this distinction is somewhat arbitrary, and we are neglecting the interaction of B with other protein atoms, but this simplest model illustrates many of the essential properties of vibrational lineshapes. Treating the protein as quasi-harmonic we write the Hamiltonian of the system as

$$H = \frac{P_B^2}{2M_B} + V_M\left(Q_B - \sum_\alpha A_\alpha \tilde{Q}_\alpha\right) + \frac{1}{2}\sum_\alpha [(d\tilde{Q}_\alpha/dt)^2 + \omega_\alpha^2 \tilde{Q}_\alpha^2] + \text{damping}, \quad \text{(D1)}$$

where P_B and Q_B are the momentum and position of atom B, respectively, and the $\{A_\alpha\}$ are coefficients that relate the position of atom A to the quasi-normal coordinates $\{\tilde{Q}_\alpha\}$. If we make a canonical transformation such that the coordinate Q_B is measured relative to $\Sigma_\alpha A_\alpha \tilde{Q}_\alpha$, which is accomplished with the operator $U = \exp\{i[\Sigma_\alpha A_\alpha \tilde{Q}_\alpha]P_B/\hbar\}$, then the dynamics of the protein and of the AB bond length decouple except for an interaction Hamiltonian

$$H_{\text{int}} = \frac{1}{2}\left(\sum_\alpha A_\alpha^2\right)P_B^2 - \left(\sum_\alpha A_\alpha \frac{d\tilde{Q}_\alpha}{dt}\right)P_B. \quad \text{(D2)}$$

If we neglect this interaction then we are making a Born-Oppenheimer, or adiabatic approximation in which the high-frequency mode is assumed to adjust its dynamics instantaneously on the time scale of protein breathing motions. Eq. D2 thus has the same form as the operator that measures the breakdown of the Born-Oppenheimmer approximation (for reviews see references 19 and 61).

Since we are primarily interested in the lineshape for infrared absorption from the ground to first excited state of the AB bond length vibrational mode we introduce the energy levels $|n\rangle$ of the Morse potential, with energies ϵ_n and fermion operators $C_n^\dagger$ and C_n which (respectively) create and annihilate molecules in the state $|n\rangle$. In terms of these operators the interaction Hamiltonian can be written as

$$H_{\text{int}} = \sum_{nm} \phi_{nm} C_n^\dagger C_m, \quad \text{(D3)}$$

where

$$\phi_{nm}(t) = \frac{1}{2}\langle n|P_B^2|m\rangle \sum_\alpha A_\alpha^2 - \langle n|P_B|m\rangle \sum_\alpha A_\alpha \frac{d\tilde{Q}_\alpha(t)}{dt}. \quad \text{(D4)}$$

The interactions of Eq. D3 can be separated into three sets. The first involves only the ground and first excited states, and it is clear that these must be kept in our analysis. The second set of terms couples the ground and excited states to the higher energy levels of the AB bond vibration, and these will be treated in perturbation theory. Finally there are terms that involve only the higher energy levels, and these are ignored as a first approximation; more precisely we include only those effects that can be described by renormalization of the Morse potential parameters.

The effective Hamiltonian which operates on the ground and first excited states is thus obtained by finding the first set of terms and adding to them the results of a perturbative calculation with terms from the second set. We use an operator form of conventional second-order perturbation theory[15] and find

$$H_{\text{int}}^{\text{eff}}(t) = \sum_{|nm|=0,1} \phi_{nm}^{\text{eff}}(t) C_n^\dagger(t) C_m(t), \quad \text{(D5)}$$

[15]This version of perturbation theory is discussed by Kittel (p. 148, reference 30).

where the effective fields are (with $\hbar = 1$)

$$\phi_{nm}^{\text{eff}}(t) = \phi_{nm}(t) - \frac{i}{2}\int_0^\infty d\tau \sum_{l\neq 0,1} [e^{-i(\epsilon_l-\epsilon_m)\tau}\phi_{nl}(t)\phi_{lm}(t-\tau) - e^{+i(\epsilon_l-\epsilon_n)\tau}\phi_{nl}(t-\tau)\phi_{lm}(t)]. \quad \text{(D6)}$$

Since the energy differences $\epsilon_n - \epsilon_l$ are of order the AB bond vibrational frequency, while the time scale for variation of $\phi_{nl}(t)$ is given by the much lower protein breathing frequency, the integral may be evaluated approximately as

$$\phi_{nm}^{\text{eff}}(t) = \phi_{nm}(t) - \sum_{l\neq 0,1}\left[\frac{\epsilon_l - (\epsilon_n+\epsilon_m)/2}{(\epsilon_l-\epsilon_n)(\epsilon_l-\epsilon_m)}\right]\phi_{nl}(t)\phi_{lm}(t). \quad \text{(D7)}$$

This defines an effective Hamiltonian for the two-level system in which the protein vibrational modes change both their average momentum and their frequencies when the local AB mode moves from the ground to the first excited state. In addition there is a matrix element between the two states that depends quadratically on the protein momenta. Since the momentum and position of a quasi-harmonic mode are approximately interchangeable, we can map this effective Hamiltonian into the same form as the phenomenological model discussed in the text provided that we restrict that model to the ground and first excited states of the high frequency mode. Specifically, the term $\sim b$ in Eq. 9 gives rise to a matrix element between the two states of the high-frequency mode, and this matrix element depends quadratically on the coordinate (which is equivalent to the momentum) of the low-frequency mode. The term $\sim c$ in Eq. 9 gives rise to a shift in equilibrium position of the low-frequency mode when the high-frequency mode is excited, which is comparable to the momentum shift found here. Of course the Hamiltonian of Eq. D7 includes some extra features, such as the shift of breathing-mode frequency upon excitation of the high frequency mode, but the rough equivalence of the two models should be clear.

To solve this model we can make use of its equivalence to models for the electronic excitation of an impurity site imbedded in a solid (52, 53). Thus in the absence of a matrix element between the two states of the high frequency mode we will see an absorption spectrum that reflects transitions from the state $|0, n\rangle$ to $|1, m\rangle$, where 0, 1 label the high-frequency mode states, as before, and n,m label the number of phonons in the breathing mode. These different transitions have energies differing by $\hbar\omega$, and hence they correspond to a collection of equally spaced lines as calculated classically in the text. When we introduce the matrix element between the states of the high-frequency mode (which is itself dependent on the coordinates of the low-frequency mode), state $|1, m\rangle$ is mixed with state $|0, m - [\Omega/\omega]\rangle$, where $[\cdots]$ denotes the integer nearest $\cdots$. This mixing of states shifts the energies of the individual $|0, n\rangle \rightarrow |1, m\rangle$ transitions by different amounts and thus spoils the equal spacing of the spectral lines. The simple pattern of equally spaced lines is further perturbed by the dependence of breathing mode frequency on the state of the high frequency mode, as noted above. More detailed calculational methods are given in reference 54.

APPENDIX E

Details of the Reaction Rate Calculation

We begin by estimating the coupling constants for the high-frequency modes associated with the iron atom and its near neighbors. A displacement Δx along a normal mode corresponds to a coupling constant $S = 2m\omega(\Delta x)^2/\hbar$, where m and ω are, respectively, the mass and frequency associated with the mode; our estimates of Δx for high-frequency localized modes are taken from the EXAFS data of reference 60, while our estimate of S for the low-frequency breathing mode is discussed in the text.

(*a*) The Fe–C stretching mode, with $\Delta x_{\text{Fe-C}} < 0.005$ nm and $\hbar\omega = 512$ cm^{-1} (65). The relevant mass is presumably the reduced mass of the Fe and CO, which determines $S < 0.4$ and a coupling energy $S\hbar\omega < 200$ cm^{-1}.

(b) The Fe–His stretching mode, with $\Delta x_{\text{Fe-His}} = 0.004 \pm 0.002$ nm and (43) $\hbar\omega \sim 220$ cm^{-1}. The relevant mass is nearly that of the iron atom, and the uncertainty in Δx is so large that we can only determine $0.3 < S < 2.6$.

(*c*) The C–O stretching mode, where no Δx data is available, and $\hbar\omega \sim 2{,}000$ cm^{-1}. A coupling $S = 1$ would require a C–O bond length change of 0.004 nm, which would be quite large considering the observed change in stretching frequency (38).

All of the data are consistent with $S < 1$, or weak coupling, for the localized modes, and so as a first approximation we shall neglect these modes in comparison with the strongly coupled low-frequency breathing mode. This approximation will have to be modified to deal with the kinetic isotope effect, as discussed in Appendix F.

The calculational methods of reference 20 are subject to two approximations. The first is slowness of the reaction compared to vibrational relaxation. Specifically, for $k_BT >> \hbar\omega$ we require $k(\omega)\,(\epsilon/k_BT)\,(E_a/k_BT) << \gamma$, where E_a is the activation energy and the other quantities are as defined in the text. The closest we come to violating this inequality is at 160 K, where the first few percent of the molecules to react may have rates too fast to be consistently calculated by our method. This does not seem to be serious, although it suggests that some care must be taken if data at higher temperatures are to be interpreted. The second requirement is the validity of perturbation theory, which is equivalent (20) to demanding that the electronic matrix element (divided by $\hbar$ to define a frequency) be larger than the rate constant. This inequality is always satisfied by many orders of magnitude.

The result of reference 20 for the reaction rate in a single-mode model is:

$$k(\omega) = \frac{4V^2}{\hbar^2}e^{-S(2\bar{n}+1)}\sum_{\mu=0}^{\infty}\sum_{\nu=0}^{\infty}\frac{[S\bar{n}]^\mu\,[S\,(\bar{n}+1)]^\nu}{\mu!\nu!} \times \frac{2\gamma\,(\mu+\nu)}{[\epsilon/\hbar - (\nu-\mu)\omega]^2 + \gamma^2\,(\nu+\mu)^2}. \quad \text{(E1)}$$

We expect that the dominant terms in this sum will come from μ and ν such that $\nu - \mu \sim \epsilon/\hbar\omega$, but at large coupling (S) this expression leads to the unphysical prediction that terms far off this resonance will dominate. This is a reflection of the long tail in the Lorentzian spectrum assumed for the vibrational modes, which corresponds to the assumption that the heat bath is equally efficient at damping arbitrarily high frequencies.

It is well known that such dissipation without cutoff does not lead to a sensible quantum theory of a damped system (61, 62) and that it is necessary to introduce some cutoff at high frequencies, or equivalently at short times in the correlation functions. We impliment this cutoff simply by multiplying the Lorentzians in Eq. E1 by Gaussians at the same central position with some width corresponding to a very short correlation time of the heat bath.

With the cutoff in place, the unphysical off-resonance terms are eliminated so long as the correlation time $\tau_c > 3 \times 10^{-14}$ s, while if $\tau_c < 10^{-10}$ s it does not affect the value of the on-resonance terms. In this regime we found that the sum in Eq. E1 could be evaluated accurately by including only terms within three neighboring resonances, i.e.,

$$[\epsilon/\hbar\omega] - 3 \leq \nu - \mu \leq [\epsilon/\hbar\omega] + 3,$$

where $[\cdots]$ denotes the integer nearest $\cdots$.

APPENDIX F

Kinetic Isotope Effects

The kinetic isotope effects in ligand binding to myoglobin might be associated with tunneling of the ligand toward the iron atom, as suggested in the initial analysis of the experiments (59). At absolute zero tunneling along the quasi-normal coordinate α inhibits the reaction rate by a factor e^{-S_α}, while the coupling constant S_α scales as the inverse one-half power of the mass associated with this coordinate. We have seen, however (Appendix E), that the coupling to localized, high-frequency vibrations of the iron atom and ligand is weak, $S_\alpha < 1$. Isotopic substitution of the C and O atoms leads, at best, to 10% changes in the effective mass and hence 5% changes in S_α. The reaction rate would then change by a factor $KIE < e^{0.05S_\alpha}$, which is <5%. With the more accurate estimates of S_α given above one finds the maximum isotope effects to be <1%, which is far too small to be consistent with experiment (59). In addition, these localized modes have $\hbar\omega_\alpha/k_B >> 160$ K, so they contribute no temperature dependence in the range of interest. The isotope effect, on the other hand, exhibits a sizable temperature dependence above ~50 K (59).

These difficulties could, in principle, be resolved by postulating some low-frequency motions of the Fe–CO complex, perhaps associated with ligand rocking in the heme pocket. To quantitatively predict the magnitude and cross-over temperature of the isotope effects, however, the frequencies would have to be so low that the zero-point motion of the ligand would correspond to essentially free tumbling and rattling in the pocket. This prediction is certainly inconsistent with the observation of well developed structure in the EXAFS spectrum of the iron atom (60) and with the sharp features of the C–O stretching vibration.

As an alternative to the tunneling picture we can try to interpret the isotope effect in terms of quantum resonances. Changes in the energy gap ϵ by $\hbar\omega \sim 20$ cm^{-1} are sufficient to take the system from one quantum resonance to the next, with large and nonmonotonic changes in the reaction rate. But the C–O stretching vibration, for example, changes frequency by ~200 cm^{-1} in the reaction, and this contributes ~ 100 cm^{-1} to the energy gap ϵ. Isotopic substitution changes the frequency by ~5%, which is enough to move from on-resonance to off-resonance, with a large decrease in reaction rate, while multiple substitutions would allow the system to climb the next peak. We thus predict a large and nonmonotonic dependence of the reaction rates on the mass of the C and O atoms, as observed (59). The resonances broaden at temperatures above $\hbar\omega/k_B \sim$ 30 K, so we expect the isotope effect to decrease above this temperature, also as observed.

The difficulty with the quantum resonance interpretation is that most of the molecules are in the relatively shallow troughs between resonances rather than on the resonant peaks themselves; in these troughs the effects associated with motion of the resonances are quite small. This suggests that resonance effects are significant only for the few percent of the molecules which have the fastest rate constants, and it is interesting that this is where the anomalous isotope effects are actually observed (59). There is also, however, a more robust interpretation of the isotope effect in terms of the energy gap law. When CO is dissociated from Fe, some bonds involving these atoms are weakened while presumably at least one (binding of the oxygen to some point in the heme pocket) is strengthened. Each of these bonds contributes to the energy gap through its change in zero-point energy during the reaction, and the contributions have different signs for the different modes. Isotopic substitution changes all of these terms, some leading to an increase of the energy gap with increasing isotopic mass, others the reverse.

The energy gap law determines an overall smooth variation of the reaction rate with energy gap and hence with isotopic masses; with the parameters of Fig. 3 this variation is certainly sufficient to account for the magnitude of the kinetic isotope effects. The nonmonotonicity is then ascribed to the competing effects of the different modes, while the temperature dependence arises because the strength of the energy gap law variations in reaction rate decreases above $\hbar\omega/k_B$ (19, 20).

Both of these effects may contribute to the observed kinetic isotope effects, and both effects predict that the isotope effect is not the same for all molecules in the ensemble. The isotope effect should therefore be time-dependent during the rebinding reaction, and observation of this time-dependence would be an important test of the theory. More detailed calculations of the isotope effect are in progress.

We thank Professor Alan Bearden for many helpful discussions regarding this work and for providing the productive environment in which much of it was carried out. Professor Hans Frauenfelder and his colleagues gave us careful instruction on their experimental results, and Professor John Hopfield informed us of his related work in advance of publication. W. Bialek also thanks the Physics Faculty of the Rijksuniversiteit Groningen for its hospitality, and R. F. Goldstein thanks the Department of Cell Biology of Stanford University for its support during a portion of this research.

Work at Berkeley was supported by the Office of Basic Energy Sciences, Office of Energy Research, U.S. Department of Energy, under contract no. AC03-76SF00098, and by the National Science Foundation Biophysics (grant no. PCM 78-22245) and Pre-Doctoral Fellowship (to W. Bialek) programs. Work at Santa Barbara was supported by the National Science Foundation under grants no. PHY77-27084 and PHY82-17853, supplemented by funds from the National Aeronautics and Space Administration. Work at Stanford was supported by the National Institutes of Health, National Institute of General Medical Sciences, under grant no. GM 24032 and by the Bank of America Giannini Post-Doctoral Fellowship program (to R. F. Goldstein).

Received for publication 15 April 1985 and in final form 17 July 1985.

REFERENCES

1. Careri, G., P. Fasella, and E. Gratton. 1979. Enzyme dynamics: the statistical physics approach. *Annu. Rev. Biophys. Bioeng.*, 8:69–97.
2. Karplus, M., and J. A. McCammon. 1981. The internal dynamics of globular proteins. *C.R.C. Crit. Rev. Biochem.* 9:293–349.
3. McCammon, J. A. 1984. Protein dynamics. *Repts. Prog. Phys.* 47:1–46.
4. Debrunner, P. G., and H. Frauenfelder. 1983. Dynamics of proteins. *Annu. Rev. Phys. Chem.* 33:283–299.
5. Austin, R. H., K. W. Beeson, L. Eisenstein, H. Frauenfelder, and I. C. Gunsalus. Dynamics of ligand binding to myoglobin. *Biochemistry.* 14:5355–5373.
6. Huber, R., and W. Bode. 1978. Structural basis of the activation and action of trypsin. *Acc. Chem. Res.* 11:114–122.
7. Beece, D., L. Eisenstein, H. Frauenfelder, D. Good, M. C. Marden, L. Reinisch, A. H. Reynolds, L. B. Sorenson, and K. T. Yue. 1980. Solvent viscosity and protein dynamics. *Biochemistry.* 19:5147–5157.
8. Salemme, F. R. 1978. Protein dynamics, potential regulation, and redox coupled conformational changes in cytochrome *c*. *In* Frontiers of Biological Energetics. I: Electrons to Tissues. P. L. Dutton, J. S. Leigh, and A. Scarpa, editors. Academic Press, Inc., New York. pp. 83–90.
9. James, M. N. G., A. R. Sielecki, G. D. Brayer, L. T. J. Delabaere, and C. A. Bauer. 1980. Structures of product and inhibitor complexes of *Streptomyces griseus* protease A at 1.8Å resolution. *J. Mol. Biol.* 144:43–88.
10. Jencks, W. P. 1969. Catalysis in Chemistry and Enzymology. McGraw-Hill Inc., New York.
11. Sturtevant, J. M. 1977. Heat capacity and entropy changes in processes involving proteins. *Proc. Natl. Acad. Sci.* USA. 74:2236–2240.
12. Dauber, P., D. J. Osguthorpe, and A. T. Hagler. 1982. Structure,

energetics and dynamics of ligand binding to dihydrofolate reductase. *Biochem. Soc. Trans.* 10:312–318.
13. Bialek, W., and R. F. Goldstein. 1983. Molecular dynamics and ligand binding in myoglobin. *Biophys. J.* 41(2, Pt. 2):221*a* (Abstr.)
14. Pines, D., editor. 1977. The Many-Body Problem. Benjamin, Reading MA.
15. Abrikosov, A. A., L. P. Gorkov, and I. E. Dzyaloshinski. 1975. Methods of Quantum Field Theory in Statistical Physics. Dover, New York.
16. Fetter, A. L., and J. D. Walecka. 1971. Quantum Theory of Many-Particle Systems. McGraw-Hill Inc., New York.
17. Doniach, S., and E. H. Sondheimer. 1974. Green's Functions for Solid State Physicists. Benjamin, Reading MA.
18. Anderson, P. W. 1984. Basic Notions of Condensed Matter Physics. Benjamin, Menlo Park CA.
19. Goldstein, R. F. 1982. Radiative and non-radiative electron transfer in photosynthesis: studies of *Chromatium vinosum*. Ph.D. thesis. University of California, Berkeley.
20. Goldstein, R. F., and W. Bialek. 1983. Vibronically coupled two-level systems: Radiationless transitions in the slow regime. *Phys. Rev. B.* 27:7431–7439.
21. von Neumann, J. 1955. Mathematical Foundations of Quantum Mechanics. Princeton University Press, Princeton NJ.
22. Goldstein, H. 1959. Classical Mechanics. Addison-Wesley, Reading MA.
23. Ziman, J. 1969. Elements of Advanced Quantum Theory. Cambridge University Press, Cambridge.
24. Noguti, T., and N. Gō. 1982. Collective variable description of small-amplitude conformational fluctuations in globular proteins. *Nature (Lond.).* 296:776–778.
25. Brooks, B., and M. Karplus. 1983. Harmonic dynamics of proteins: normal modes and fluctuations in bovine pancreatic trypsin inhibitor. *Proc. Natl. Acad. Sci. USA.* 80:6571–6575.
26. Laubereau, A. 1979. Picosecond Raman scattering. *Phil. Trans. Roy. Soc. Lond. A.* 293:441–453.
27. Phillips, S. E. V. 1980. Structure and refinement of oxymyoglobin at 1.6Å resolution. *J. Mol. Biol.* 142:531–554.
28. Blake, C. C. F., W. C. A. Pulford, and P. J. Artymiuk. 1983. X-ray studies of water in crystals of lysozyme. *J. Mol. Biol.* 167:693–723.
29. Middendorf, H. D., and J. Randall. 1980. Molecular dynamics of hydrated proteins. *Phil. Trans. Roy. Soc. Lond. B.* 290:639–654.
30. Kittel, C. 1963. Quantum Theory of Solids. John Wiley & Sons, New York.
31. Levy, R. M., and M. Karplus. 1979. Vibrational approach to the dynamics of an alpha helix. *Biopolymers.* 18:2465–2495.
32. Randall, J., and J. M. Vaughn. 1979. Brillouin scattering in systems of biological importance. *Phil. Trans. Roy. Soc. Lond. A.* 293:341–347.
33. Nagai, K., T. Kitagawa, and H. Morimoto. 1980. Quaternary structures and low frequency molecular vibrations of haems in deoxy and oxyhaemoglobin studied by resonance Raman scattering. *J. Mol. Biol.* 136:271–289.
34. Parak, F., E. N. Frolov, R. L. Mössbauer, and V. I. Goldanskii. 1981. Dynamics of metmyoglobin crystals investigated by nuclear gamma resonance absorption. *J. Mol. Biol.* 145:825–833.
35. Parak, F., E. W. Knapp, and D. Kucheida. 1982. Protein dynamics: Mössbauer spectroscopy on deoxymyoglobin crystals. *J. Mol. Biol.* 161:177–194.
36. Knapp, E. W., S. F. Fischer, and F. Parak. 1983. The influence of protein dynamics on Mössbauer spectra. *J. Chem. Phys.* 78:4701–4711.
37. Bauminger, E. R., S. G. Cohen, I. Nowick, S. Ofer, and J. Yariv. 1983. Dynamics of iron in crystals of metmyoglobin and deoxymyoglobin. *Proc. Natl. Acad. Sci. USA.* 80:736–740.
38. Alben, J. O., D. Beece, S. F. Bowne, W. Doster, L. Eisenstein, H. Frauenfelder, D. Good, J. D. McDonald, M. C. Marden, P. P. Moh, L. Reinisch, A. H. Reynolds, E. Shyamsunder, and K. T. Yue. 1982. Infrared spectroscopy of photodissociated carboxymyoglobin at low temperature. *Proc. Natl. Acad. Sci. USA.* 79:3744–3748.
39. Morse, P. M. 1929. Diatomic molecules according to the wave mechanics. II. Vibrational levels. *Phys. Rev.* 34:57–64.
40. Rousseau, D. L., and M. R. Ondrias. 1983. Resonance Raman scattering studies of the quaternary structure transition in hemoglobin. *Annu. Rev. Biophys. Bioeng.* 12:357–380.
41. Hendrikson, W. A., and J. Konnert. 1981. *In* Biomolecular Structure, Function, Conformation, and Evolution. I. R. Srinivasan, editor. Pergamon Press, Ltd., Oxford.
42. Gavish, B. 1981. Modeling the unusual temperature dependence of atom displacements in proteins by local non-harmonic potentials. *Proc. Natl. Acad. Sci. USA.* 78:6868–6872.
43. Kitagawa, T., K. Nagai, and M. Tsubaki. 1979. Assignment of the Fe–N_ϵ (His F8) stretching band in the resonance Raman spectra of deoxy myoglobin. *FEBS (Fed. Eur. Biochem. Soc.) Lett.* 104:376–378.
44. Desbois, A., M. Lutz, and R. Banerjee. 1979. Low-frequency vibrations in resonance Raman spectra of horse heart myoglobin. Iron-ligand and iron-nitrogen vibrational modes. *Biochemistry.* 18:1510–1518.
45. Frauenfelder, H., G. A. Petsko, and D. Tsernoglou. 1979. Temperature-dependent x-ray diffraction as a probe of protein structural dynamics. *Nature (Lond.).* 280:558–563.
46. Perutz, M. F., S. S. Hasnain, P. J. Duke, J. L. Sessler, and J. E. Hahn. 1982. Stereochemistry of iron in deoxyhaemoglobin. *Nature (Lond.).* 295:535–538.
47. Theroell, H., and A. Ehrenberg. 1951. Spectrophotometric, magnetic and titrimetric studies on the heme-linked groups in myoglobin. *Acta Chem. Scand.* 5:823–848.
48. Nakano, N., J. Otsuka, and A. Tasaki. 1971. Fine structure of iron ion in deoxymyoglobin and deoxyhemoglobin. *Biochem. Biophys. Acta.* 236:223–233.
49. Kubo, R. 1952. Thermal ionization of trapped electrons. *Phys. Rev.* 86:929–937.
50. Freed, K. F., and J. Jortner. 1970. Multiphonon processes in the nonradiative decay of large molecules. *J. Chem. Phys.* 52:6272–6291.
51. Soules, T. F., and C. B. Duke. Resonant energy transfer between localized electronic states in a crystal. *Phys. Rev. B.* 3:262–274.
52. Huang, K. 1981. Lattice relaxation and multi-phonon transitions. *Contemp. Phys.* 22:599–612.
53. Stoneham, A. M. 1981. Non-radiative transitions in semiconductors. *Repts. Prog. Phys.* 44:1251–1295.
54. Bialek, W. 1983. Quantum effects in the dynamics of biological systems. Ph.D. thesis, University of California, Berkeley.
55. Englman, R. 1979. Non-Radiative Decay of Ions and Molecules in Solids. Elsevier/North-Holland, Amsterdam.
56. Friedman, J. M., and T. W. Scott. 1983. Fluorescence line narrowing (FLN) of the tryptophan emission in adult human hemoglobin. *Bull. Am. Phys. Soc.* 28:403.
57. Goldstein, R. F., and W. Bialek. Protein dynamics and reaction rates: Are simple models useful? *Comments Mol. Cell. Biophys.* In press.
58. Frauenfelder, H. 1984. Ligand binding and protein dynamics. *In* Structure and Dynamics of Nucleic Acids, Proteins, and Membranes. E. Clementi and R. H. Sarma, editors. Adenine Press, New York.
59. Alben, J. O., D. Beece, S. F. Bowne, L. Eisenstein, H. Frauenfelder, D. Good, M. C. Marden, P. P. Moh, L. Reinisch, A. H. Reynolds, and K. T. Yue. 1980. Isotope effect in molecular tunneling. *Phys. Rev. Lett.* 44:1157–1160.

60. Powers, L. 1982. X-ray absorption spectroscopy. Application to biological molecules. *Biochim. Biophys. Acta.* 683:1–38.
61. Caldeira, A. O., and A. J. Leggett. 1983. Quantum tunneling in a dissipative system. *Ann. Phys.* 149:374–456.
62. Caldeira, A. O., and A. J. Leggett. 1983. Path integral approach to quantum Brownian motion. *Physica.* 121A:587–616.
63. Landau, L. D., and E. M. Lifshitz. 1977. Statistical Physics. Pergamon Press, Ltd., Oxford.
64. Lovesey, S. 1980. Condensed Matter Physics: Dynamic Correlations. Benjamin, Reading MA.
65. Tsubaki, M., R. B. Srivastava, and N.-T. Yu. 1982. Resonance Raman investigation of carbon monoxide bonding in (carbonmonoxy)hemoglobin and -myoglobin: detection of Fe–CO stretching and Fe–C–O bending vibrations and influence of quaternary structure change. *Biochemistry.* 21:1132–1140.